

2020-01-01

## The Dynamic Transition of a Vertical Take-Off and Landing Drone

Luis Carlos Calvo Jr.  
*University of Texas at El Paso*

Follow this and additional works at: [https://scholarworks.utep.edu/open\\_etd](https://scholarworks.utep.edu/open_etd)



Part of the [Mechanical Engineering Commons](#)

---

### Recommended Citation

Calvo Jr., Luis Carlos, "The Dynamic Transition of a Vertical Take-Off and Landing Drone" (2020). *Open Access Theses & Dissertations*. 3147.

[https://scholarworks.utep.edu/open\\_etd/3147](https://scholarworks.utep.edu/open_etd/3147)

This is brought to you for free and open access by ScholarWorks@UTEP. It has been accepted for inclusion in Open Access Theses & Dissertations by an authorized administrator of ScholarWorks@UTEP. For more information, please contact [lweber@utep.edu](mailto:lweber@utep.edu).

THE DYNAMIC TRANSITION OF A VERTICAL TAKE-OFF AND LANDING DRONE

LUIS CARLOS CALVO JR.

Doctoral Program in Mechanical Engineering

APPROVED:

---

Louis Everett, Ph.D., Chair

---

Angel Flores-Abad, Ph.D.

---

Methaq Abed, Ph.D.

---

Patricia Nava, Ph.D.

---

Stephen L. Crites, Jr., Ph.D.  
Dean of the Graduate School

Copyright ©

by

Luis Carlos Calvo Jr.

2020

## **Dedication**

I would like to dedicate this to my family and loved ones for always supporting me in the decisions I've made to get me where I am today.

THE DYNAMIC TRANSITION OF A VERTICAL TAKE-OFF AND LANDING DRONE

by

LUIS CARLOS CALVO JR., B.S.M.E, M.S.M.E

DISSERTATION

Presented to the Faculty of the Graduate School of

The University of Texas at El Paso

in Partial Fulfillment

of the Requirements

for the Degree of

DOCTOR OF PHILOSOPHY

Department of Mechanical Engineering

THE UNIVERSITY OF TEXAS AT EL PASO

December 2020

## **Acknowledgments**

I would like to thank my loved ones for all of the support given to me to accomplish this amazing milestone. I would especially like to thank my advisors, Dr. Michael McGee and Dr. Louis Everett, for giving me this opportunity and amazing guidance throughout the past years. I could not have made it without everyone mentioned, and I am extremely grateful.

## **Abstract**

Unmanned aerial vehicles, or UAVs, are small pilotless aircrafts that are remotely controlled through a ground control station. They have increased in popularity because of their applications and the advantages that each UAV can provide based on their need. There are many types of UAVs, but this study focuses on a type of Vertical Take-Off and Landing (VTOL) UAV that is known as the Albatross UAV. This UAV was manufactured by a company known as Applied Aeronautics, and configurations were made to change the fixed-wing (FW) UAV to a VTOL UAV. This study was done to find methodologies to simulate different dynamic transitions of the Albatross UAV from hover to FW flight and from FW flight back to hover using MATLAB. Those simulations were then used to compare the transitions done from the Dronecode flight control software. Speed, efficiency, and altitude gain/loss will be compared from these transitions.

## Table of Contents

Dedication .....	iii
Acknowledgments.....	v
Abstract.....	vi
Table of Contents .....	vii
List of Tables .....	ix
List of Figures .....	x
Chapter 1: Introduction.....	1
Chapter 2: Rationale .....	7
2.1 Importance .....	7
2.1.1 Applications .....	7
2.1.2 Hover to Fixed-Wing Transitions .....	9
2.1.3 Fixed-Wing to Hover Transitions .....	11
Chapter 3: Literature Review.....	12
3.1 Hover Study .....	12
3.2 Hover to Fixed-Wing Flight Study .....	14
3.3 Fixed-Wing Flight Study .....	18
3.4 Fixed-Wing to Hover Study.....	22
3.5 Stall .....	23
Chapter 4: Methodology .....	25
4.1 Calculations.....	25
4.2 Algorithm.....	30
4.3 Testing.....	30

Chapter 5: Results and Discussion.....	32
5.1 Hover to Fixed-Wing Transitions .....	32
5.1.1 Baseline Transition (No Altitude Loss) .....	32
5.1.2 Flat Level Transition (Same Initial/Desired Altitude).....	38
5.1.3 Pitched-Back Transition (No Altitude Loss) .....	43
5.1.4 Pitch-Forward Transition (No Altitude Loss).....	47
5.1.5 Flat Free-Fall Transition (Decrease in Altitude).....	51
5.1.6 Nose-Dive Transition (Decrease in Altitude) .....	55
5.2 Fixed-Wing to Hover Transitions .....	60
5.2.1 Reverse Thrust Transition.....	60
5.2.2 Flat Gliding Transition.....	65
5.2.3 Pitched-Back Gliding Transition .....	70
Chapter 6: Conclusion.....	74
References.....	78

Vita 83

## List of Tables

Table 3.1: Hover Motor and Propeller Selection .....	14
Table 3.2: Albatross UAV Parameters.....	19
Table 6.1: Hover to Fixed-Wing Transition Comparison.....	76
Table 6.2: Fixed-Wing to Hover Transition Comparison.....	77

## List of Figures

Figure 1.1: Quadrotor UAV (Jamal, 2018).....	1
Figure 1.2: Fixed-Wing UAV (Albatross Airframe, n.d.) .....	2
Figure 1.3: Tilt-Rotor UAV (Jin-seo, 2007).....	3
Figure 1.4: Tilt-Wing UAV (Masuda & Uchiyama, 2018) .....	3
Figure 1.5: Tail-Sitter UAV (Zhang, Chen, & Lv, 2012).....	4
Figure 1.6: Vertical Take-Off and Landing Fixed Wing UAV (Cakici & Leblebicioglu, Analysis of a UAV that can Hover and Fly Level, 2016).....	4
Figure 1.7: VTOL-FW UAV X-Way Fixed Bar (Cakici & Leblebicioglu, 2016).....	6
Figure 1.8: VTOL-FW UAV 11-Way Fixed Bar (Yu & Kwon, 2017).....	6
Figure 2.1: Infrared Surveillance (Can Thermal Imaging See Through Walls? And Other Common Questions, 2020) .....	8
Figure 2.2: Traffic Response (Who's at Fault in a Multi-Car Accident?, 2018).....	8
Figure 2.3: Agricultural Maintenance (Kloosterman, et al., 2019).....	9
Figure 2.4: VTOL-FW Transition Method (Collins, 2020).....	10
Figure 3.1: Hover Rotor Location/Rotation (Quadplane Configuration, n.d.) .....	13
Figure 3.2: Transition Controls (Cakici & Leblebicioglu, 2016) .....	15
Figure 3.3: Critical Angle of Attack (AOA) (Airfoil Tools, n.d.) .....	16
Figure 3.4: Quadplane Transition (Cakici & Leblebicioglu, 2016).....	17
Figure 3.5: Quadplane vs. Tilt-Rotor Pitch Angle Comparison (Govdel, Muzaffae, Raj, Elhadidi, & Kayacan, 2019). .....	18
Figure 3.6: AOA vs Drag Coefficient (Sogukpinar & Bozkurt, 2015).....	20
Figure 3.7: AOA vs Lift to Drag Ratio (Sogukpinar & Bozkurt, 2015).....	21

Figure 3.8: Albatross UAV Lift to Drag Ratio .....	21
Figure 3.9: Perching Tail-Sitter UAV (Marchini, 2013) .....	22
Figure 3.10: Quadplane vs. Tilt-Rotor Pitch Angle Comparison (Govdel, Muzaffae, Raj, Elhadidi, & Kayacan, 2019).....	23
Figure 4.1: Inertial Reference Frame (Basson, 2010).....	28
Figure 4.2: Body Reference Frame (Basson, 2010).....	28
Figure 4.3: Forces on an Aircraft (Forces in a Climb, n.d.).....	29
Figure 5.1: Baseline Transition Forces .....	35
Figure 5.2: Baseline Transition Velocities.....	36
Figure 5.3: Baseline Transition Positions .....	37
Figure 5.4: Flat Level Transition Forces.....	40
Figure 5.5: Flat Level Transition Velocities .....	41
Figure 5.6: Flat Level Transition Positions .....	42
Figure 5.7: Pitched-Back Transition Forces .....	44
Figure 5.8: Pitched-Back Transition Velocities.....	45
Figure 5.9: Pitched-Back Transition Positions .....	46
Figure 5.10: Pitched-Forward Transition Forces .....	48
Figure 5.11: Pitched-Forward Transition Velocities .....	49
Figure 5.12: Pitched-Forward Transition Positions .....	50
Figure 5.13: Flat Free-Fall Transition Forces .....	52
Figure 5.14: Flat Free-Fall Transition Velocities .....	53
Figure 5.15: Flat Free-Fall Transition Positions .....	54
Figure 5.16: Nose-Dive Transition Forces.....	57

Figure 5.17: Nose-Dive Transition Velocities .....	58
Figure 5.18: Nose-Dive Transition Positions.....	59
Figure 5.19: Reverse Thrust Transition Forces.....	62
Figure 5.20: Reverse Thrust Transition Velocities.....	63
Figure 5.21: Reverse Thrust Transition Positions.....	64
Figure 5.22: Flat Gliding Transition Forces .....	67
Figure 5.23: Flat Gliding Transition Velocities.....	68
Figure 5.24: Flat Gliding Transition Positions .....	69
Figure 5.25: Pitched-Back Gliding Transition Forces .....	71
Figure 5.26: Pitched-Back Gliding Transition Velocities.....	72
Figure 5.27: Pitched-Back Gliding Transition Positions .....	73

## Chapter 1: Introduction

Unmanned aerial vehicles (UAVs) are small pilotless aircrafts that are remotely controlled through a ground control station. In recent years, the use of UAVs has increased and gained popularity because of their applications, such as law enforcement surveillance, being able to carry payloads for the military, traffic monitoring, and even agricultural maintenance. There are various types of UAVs to perform these actions, such as a quadrotor (Figure 1.1), fixed-wing (Figure 1.2), tilt-rotor (Figure 1.3), tilt-wing (Figure 1.4), tail-sitter (Figure 1.5), and vertical take-off and landing fixed-wing (VTOL-FW) (Figure 1.6), also known as a Quadplane.

Each of these UAV designs has its advantages and disadvantages based on need and application. The quadrotor is the most common of the UAVs, with four hover rotors used to maneuver the UAV. Even though it may not cover a large distance in a short amount of time, the design allows for easier control such as indoor environments (Guo & Horn, 2012). The quadrotor is also able to hover and land in more confined areas and switch direction of flight with ease.



Figure 1.1: Quadrotor UAV (Jamal, 2018)

A fixed-wing (FW) UAV is like a small aircraft that still requires a runway to take off and land. One of the main advantages of this UAV is that it is able to cover large distances at higher velocities. However, there is more difficulty controlling this specific type of UAV when wanting to land it in more confined areas, especially if a runway is not available. Another issue that occurs with FW UAVs is the path-following problem that is determined by the initial location of the vehicle and its heading angle (Sujit, Saripalli, & Sousa, 2014).



Figure 1.2: Fixed-Wing UAV (Albatross Airframe, n.d.)

Both tilt-rotor and tilt-wing require complicated software and hardware such as actuators, gearboxes, and extra servos (Apkarian, 2017) to increase drag and the total weight of the UAV. However, they have the capability to remove the need for a runway to take off. This also allows for both the tilt-rotor and tilt-wing to hover in hard to reach areas when needed.



Figure 1.3: Tilt-Rotor UAV (Jin-seo, 2007)

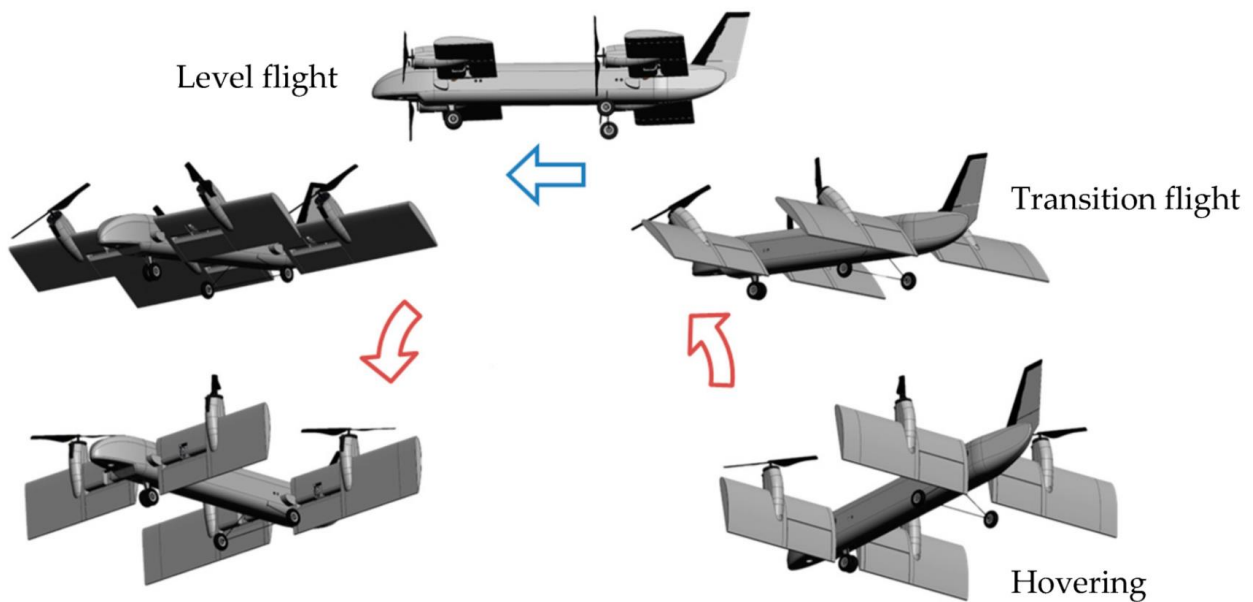


Figure 1.4: Tilt-Wing UAV (Masuda & Uchiyama, 2018)

The tail-sitter UAV has a complicated control system and is more vulnerable to the wind (Dundar, Bilici, & Unler, 2020) compared to other previously mentioned UAVs. Although not as easy to maneuver as a quadrotor, it is still given the advantage of hover around a specific location when needed and take-off and land in a wider variety of location.



Figure 1.5: Tail-Sitter UAV (Zhang, Chen, & Lv, 2012)



Figure 1.6: Vertical Take-Off and Landing Fixed Wing UAV (Cakici & Leblebicioglu, Analysis of a UAV that can Hover and Fly Level, 2016)

The topic of research for this project is to find different methodologies for the dynamic transition of a vertical take-off and landing fixed-wing (VTOL-FW) UAV known as the Albatross PX4. This specific UAV is a fixed-wing (FW) aircraft like other airliners capable of flight using their wings to generate lift. For the Albatross UAV, configurations were made to change and

simulate the drone from FW to VTOL-FW using MATLAB. The need for the UAV to use a runway to obtain lift will be removed, through these changes. As the name suggests, the VTOL-FW UAV will obtain flight by hovering, transitioning to fixed-wing flight, and transitioning back to hover. This capability will allow the UAV to attain flight in environments such as caves for low altitudes, forests where runway space is unavailable, and rural areas. With this VTOL-FW design, the UAV will be given the advantage of having the maneuverability of a helicopter (Whalley, 1991), enabling stable hover whenever necessary, and the ability to act as a quadcopter for control in confined spaces. The Albatross UAV will also still have the endurance of a plane to achieve longer distances than a standard quadcopter because of its FW capability.

The focus of this study was to do various types of dynamic transitions from hover to fixed-wing flight and back to hover of the VTOL-FW UAV, along with doing the standard transition that is commonly used with the Dronecode flight control software. These different methods were tested using different initial conditions and recorded to compare and conclude which transition is most useful depending on the environment and situation. From the data that was recorded, the comparison of the most efficient transition to preserve battery life was investigated because with each transition that is made, there is going to be power drained from the battery (Dundar, Bilici, & Unler, 2020). Speed was also investigated to determine which is the fastest transition in the case of emergencies and speedy departures.

From research on design perspectives, two designs of the Quadplane were investigated. The first being the X-Way Fixed Bar (Yu & Kwon, 2017) (Figure 1.8). This design is generally used for most VTOL drones. However, based on this project's current goals, the X-Way Fixed Bar method would not be ideal. This is due to the increase in the total weight of the Albatross drone because of the need for additional equipment used to stabilize the bars, in turn affecting the

maneuverability. The other design method studied was known as the 11-Way Fixed Bar (Yu & Kwon, 2017) (Figure 1.9). This method does not need as much additional support or equipment, and the drag is relatively small because of the arms being parallel to each other and not creating as much surface area for the FW flight. This parallel design will assist with the efficiency of the transitions that are studied. Therefore, the 11-way method is the most advantageous and was pursued for this research.



Figure 1.7: VTOL-FW UAV X-Way Fixed Bar (Cakici & Leblebicioglu, 2016)



Figure 1.8: VTOL-FW UAV 11-Way Fixed Bar (Yu & Kwon, 2017)

## **Chapter 2: Rationale**

### **2.1 Importance**

The importance of this study is to determine different methodologies of the VTOL UAV to be able to transition from hover to FW flight and from FW flight back to hover. Compare them to the baseline transitions that are standard in the UAS industry and is the standard transition used in Ardupilot and Dronecode flight control software. It was investigated to see if there would be a more efficient transition, a speedier transition, and even transitions that would be most advantageous based on different scenarios. Initially, the transitions from hover to FW flight were studied and compared, then the transitions from FW flight to hover were studied.

#### **2.1.1 Applications**

Initially, design and simulations were made for the White Sands Missile Range (WSMR). Through this, the many uses for the VTOL-FW UAV, including having the capability of being used for surveillance. The UAV would attach a flat mapping gimbal that keeps a camera parallel to the ground for a wide range of surveillance and mission usages. An important use of the gimbal would include law enforcement surveillance. An example would be infrared surveillance that could be useful when searching for missing persons (Figure 2.1). When the drone is in FW mode, it would cover a great distance during the search. The Remote Pilot in Command (RPIC) would then be able to transition to hover mode to have better control of the UAV and pin-point the location with live feed.



Figure 2.1: Infrared Surveillance (Can Thermal Imaging See Through Walls? And Other Common Questions, 2020)

As far as traffic emergencies (Figure 2.2), the VTOL-FW UAV will be able to reach the area of an accident sooner and faster than a ground vehicle and convey information and visualize the magnitude of the accident. This information is also useful to redirect traffic to assist incoming emergency units responding to the issue, making the response as efficient as possible.



Figure 2.2: Traffic Response (Who's at Fault in a Multi-Car Accident?, 2018)

Another use of the VTOL-FW drone is for agricultural maintenance (Figure 2.3). Farmers can use the drone to conduct soil and field analysis providing data for irrigation and nitrogen-level management. Planting by achieving a higher uptake rate, decreasing planting costs, crop spraying, and crop monitoring with increased efficiency. The drone can also be used for irrigation and health assessment with thermal sensors to identify parts of a field that are dry and need improvements.



Figure 2.3: Agricultural Maintenance (Kloosterman, et al., 2019)

### **2.1.2 Hover to Fixed-Wing Transitions**

The baseline transition that is normally done through the Dronecode flight control software (Flying a Quadplane, n.d.) that was tested was done by preventing any altitude loss during the transition. Another transition was a flat level transition of steady hover to FW flight by simply

initiating the FW rotor to begin the transition without any change to the initial or desired conditions other than the desired velocity. With two other transitions that were done, the first of the two, before turning on the FW rotor was to pitch the drone back (Figure 2.4a) for a higher initial angle of attack to increase the amount of lift from the wing when thrust is being applied in the forward direction by the FW rotor. A minor force is provided in the negative x-direction because of pitching the UAV back by a certain amount, but not enough to provide a retarding force. This method is done to create a transition from hover to FW flight with the max allowable AOA just below the critical AOA. The second of the two was essentially the opposite. With this method, the drone was pitched forward (Figure 2.4b) since the wings are initially pitched back by  $7^\circ$  when the edrone's fuselage is pitched at  $0^\circ$ , to see if this would decrease the total amount of time for the transition to take place. There will still be lift being provided from the wings since this transition is done by using the Optimum AOA. Both were simulated to not lose any altitude while the transition is taking place.

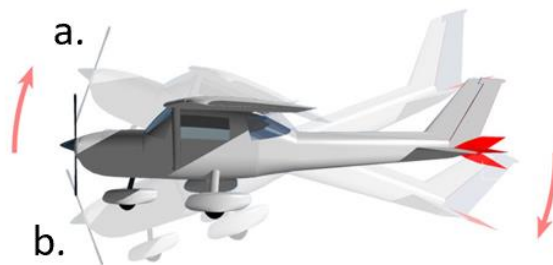


Figure 2.4: VTOL-FW Transition Method (Collins, 2020)

Two other types of transitions were tested at altitudes high enough to where it would be possible to shut off the hover rotors to allow for a free fall. The first transition is based on the theory that once the altitude is reached, a nose-dive will be obtained, similar to what is known as

Kvochur's Bell (Bushgens & Sukhanov, 2018), and turn on the FW rotor to initiate the transition. The difference between this transition and Kvochur's Bell is the the UAV will be hovering steady at an altitude high enough, and then begin a nose-dive to begin the transition. This was done to see if falling from a high altitude would assist the UAV to transition at a faster speed. The second would begin in a similar fashion where once the drone is at an altitude high enough, the hover rotors would once again be shut off to begin somewhat of a flat free-fall (Kim, Oh, Seo, & Kim, 2017) of the drone. This will be done without the spin, but once ready, turn on the FW rotor to initiate the transition from hover to FW flight. This specific transition was done in any case the Remote Pilot in Command (RPIC) is no longer able to hover, a transition would be able to take place to switch from hover mode to fixed-wing (FW) mode. Each of these transitions is possible for a tilt-rotor and tilt-wing UAV but limited on a tail-sitter UAV because of its unique design.

### **2.1.3 Fixed-Wing to Hover Transitions**

Just like the hover to fixed-wing transitions, different fixed-wing to hover transitions from FW flight to hover were tested and compared. The first backwards transition was to have the UAV flying at a specific velocity, and the FW rotor will then begin to produce a reverse thrust while simultaneously turning on the hover rotors to prepare for the hover mode to completely take over. The second begins with shutting off the FW rotors and slowly turning on the hover rotors to see how long it would take to fully have control with the four hover rotors from letting the UAV glide through the air. The last will start in a similar fashion of shutting off the FW rotor to allow the UAV to glide and turning on the hover rotors to create a backward pitch of  $4^\circ$  to get an Angle of Attack (AOA) of  $11^\circ$ , right under the value of the Critical Angle of Attack (AOA) to prevent a stall.

## **Chapter 3: Literature Review**

There are various uses and advantages to having a VTOL-FW UAV at your disposal such as not needing a runway, being able to hover for precise location, or be in FW mode to cover long distances. However, some disadvantages could occur and the objective is to be able to have a solution that overcomes those disadvantages.

### **3.1 HOVER STUDY**

Quadcopter UAVs were investigated to best study how the design and hover of the Albatross UAV will take place. These are simply designed UAVs with four rotors spaced out evenly from the Center of Gravity (COG) of a body. The first items investigated were the placement and rotation of the four hover rotors. Because of the way the Albatross UAV was manufactured, the four hover rotors were each placed 40 inches apart from each other using 2x2 twill weave carbon fiber structural components located in between where the wings come apart. With an equal number of the propellers spinning in opposite directions, the torques created from the spin would be able to cancel out and not cause the UAV to yaw in one direction or another while in hover mode (Figure 3.1) (Dydek, Annaswamy, & Lavretsky, 2013). The placement of the motors and propellers were placed at an equal distance from the COG to prevent any cause of COG variations (Lee, Giri, & Son, 2017).

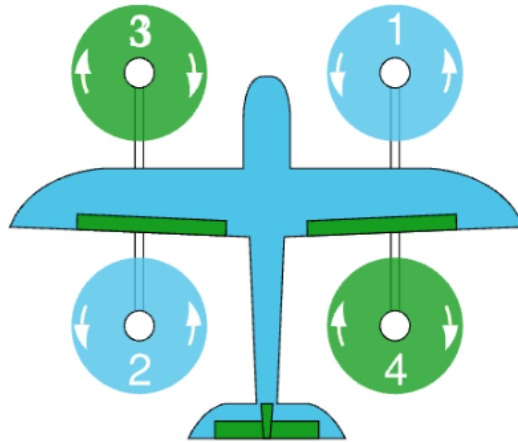


Figure 3.1: Hover Rotor Location/Rotation (Quadplane Configuration, n.d.)

For these unmanned aircrafts, brushless motors are typically what is used for various applications because they provide an additional control loop that significantly improves the performance of the attitude stability (Sanchez, Carrillo, Rondon, Lozano, & Garcia, 2010). Considering the size of the Albatross UAV for this simulation, and the applications it will be used for, the motors and propellers were carefully selected for use.

Table 3.1: Hover Motor and Propeller Selection

Motor Version	Propeller Size	Throttle Range	Amperage (A)	Power Input (W)	Thrust Output (lb.)	RPM (rev/min)
KDE4215XF-465	18.5' x 6.3 KDE- CF185- DP DUAL- BLADE	25.0%	3.0	69	1.85	2760
		37.5%	7.0	161	3.62	3840
		50.0%	13.0	300	5.45	4740
		62.5%	22.0	508	7.69	5640
		75.0%	34.0	785	9.85	6363
		87.5%	49.2	1136	12.24	7200
		100.0%	68.6	1584	15.65	7860

From these selections, the total amount of thrust output from the four combined at 100% throttle will be 62.6 lbs. Therefore, since the weight of the drone is to be maxed out at 55 lbs., the addition of a payload or gimbal would not be an issue.

### 3.2 HOVER TO FIXED-WING FLIGHT STUDY

One of the more focused portions of this study is the transition. A tail-sitter UAV was able to achieve a transition from hover to fixed wing flight in a short amount of time by using slats and flaps (Kubo, 2006). Other previous studies mention the use of tumble-stall maneuvers, dynamic inversion methods, and backstepping control techniques (Cakici & Leblebicioglu, 2016). For this project, the transition of a Quadplane was studied to create unique but effective, hybrid transitions that are applicable in different scenarios.

One aspect was the control of the drone while in transition. For this Quadplane, there are essentially two different controllers. One for the hover, and one for the FW flight. Instead of a direct shut off from one control to the other, the controls intersect and are all active during the transition. During hover mode, the hover controls are active. This would tell the UAV to roll, pitch, or yaw accordingly with the four hover rotors. During transition mode, the FW controls activate turning on the FW rotor, but the hover control elements do not shut off immediately. For the FW control to completely take over, the UAV must reach the desired speed so that the wings produce a lift of 22 lbs. The hover rotors will be able to completely shut off, and FW mode is in full control. This is a default value for the UAV within the Ground Control Station (GCS). That value could be left as is or changed to a different desired value if need be. A perfect example is shown in Figure 3.2 from (Cakici & Leblebicioglu, 2016) ,which shows at what point each controller is active individually and simultaneously,which allows for a smoother transition during the process.

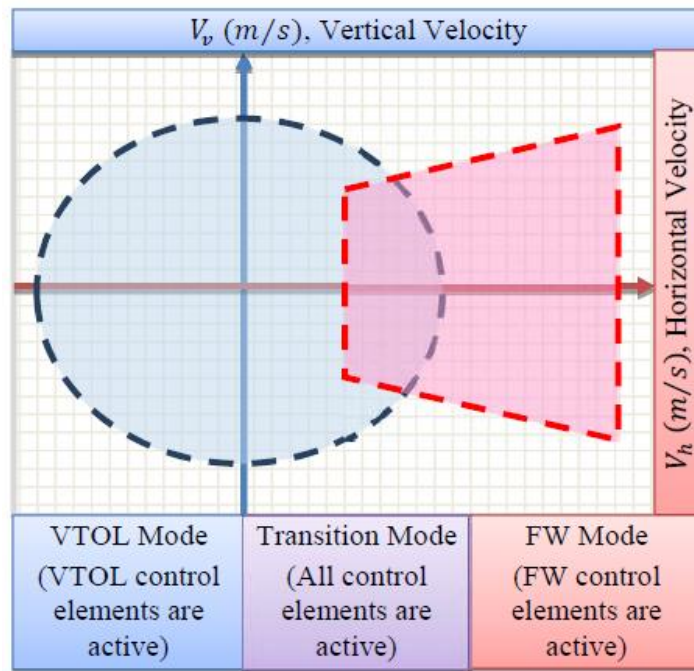


Figure 3.2: Transition Controls (Cakici & Leblebicioglu, 2016)

During the transition, lift from the wings is produced and then used for an aircraft to take off and either gain altitude or remain at the desired altitude. The greater the Angle of Attack (AOA), the greater the amount of lift that will be produced up to a certain point, which is known as the Critical AOA. When past the point of Critical AOA, the stall will begin to occur. For the Albatross UAV and the type of airfoil used, the Critical AOA is at  $11.25^\circ$  (Figure 3.3).

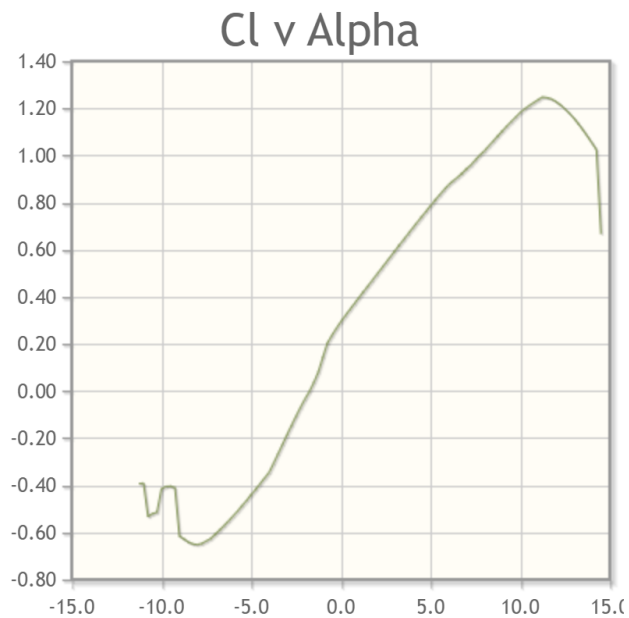


Figure 3.3: Critical Angle of Attack (AOA) (Airfoil Tools, n.d.)

When grounded, the wings of the Albatross UAV are already at an AOA of  $7^\circ$ . However, since the drone will already be hovering and will have no need for a runway, the transition is possible at a lower AOA. It is easier to control what is needed from the UAV while in hover mode because the drone's pitch is one of the main controlling factors during the transition. The reason a lower AOA would take place and not a value of  $0^\circ$  is that during the transition, the drone still tends to drop in altitude (Cakici & Leblebicioglu, 2016) (Figure 3.4). The UAV will descend

because originally, the four hover rotors are what is keeping it at a specific altitude. During the transition, the hover rotors will at one point shut off, and the UAV will descend a bit until enough lift is created from the wing to have the UAV ascend again. For some of the applications in this study, such as being able to transition in lower altitudes when needed, a descend during transition is not ideal. In contrast, in other applications, perhaps a great amount of lift is needed to ascend to greater heights at higher speeds.

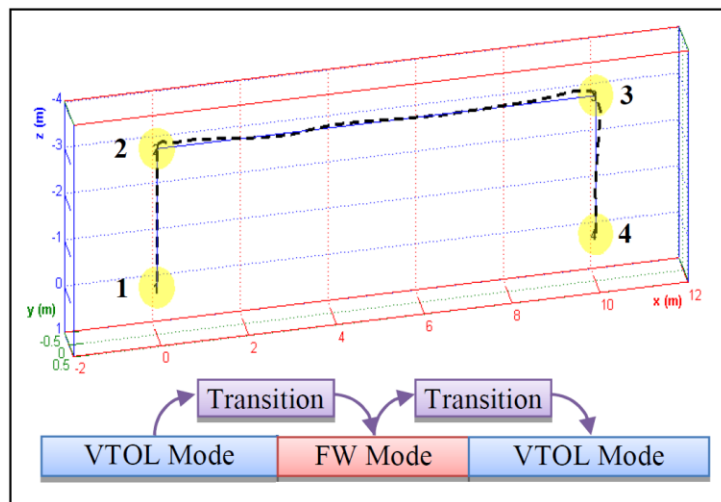


Figure 3.4: Quadplane Transition (Cakici & Leblebicioglu, 2016)

From previous works of literature, there are very few studies on Quadplanes that have focused on the transition from hover to FW flight. Those that have studied the transition mainly compare the results of a Quadplane UAV to a tilt-rotor or tilt-wing (Govdel, Muzaffae, Raj, Elhadidi, & Kayacan, 2019). The image below (Figure 3.5) shows the comparison of pitch between a Quadplane and a tilt-rotor. From here, it is seen that only a  $2^\circ$  change in pitch was needed for the tilt-rotor UAV to complete the transition from hover to FW flight. Other studies show the transition

is only needing about 3° degrees to complete the transition as well (Yukse, Vuruskan, Ozdemir, Yukselen, & Inalhan, 2016), showing that not too much of a pitch is needed.

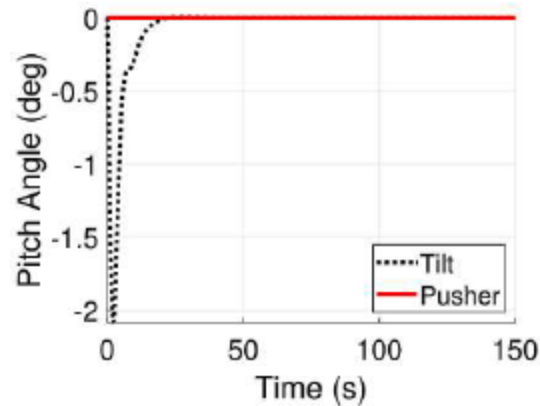


Figure 3.5: Quadplane vs. Tilt-Rotor Pitch Angle Comparison (Govdel, Muzaffae, Raj, Elhadidi, & Kayacan, 2019).

### 3.3 FIXED-WING FLIGHT STUDY

In this study, the Albatross UAV was originally a FW UAV before configurations were made to convert the UAV to a Quadplane. Studying the UAV in its FW state was done to better simulate the transitions. Table 3.2 states the parameters used to assist with the calculations done for FW flight.

Table 3.2: Albatross UAV Parameters

Airfoil Type		NACA-2412
Wingspan		9.8425 ft.
Wing Area		8 ft. <sup>2</sup>
Weight of Drone		22 lbs.
Reynold's Number		~250,000
Mean Aerodynamic Chord		0.8125 ft.
Density		0.063177 lb./ft. <sup>3</sup>
Moments of Inertia	Ixx	2.43E11 lb./ft. <sup>2</sup>
	Iyy	1.71E11 lb./ft. <sup>2</sup>
	Izz	3.84E11 lb./ft. <sup>2</sup>
Propeller	Diameter	14 in.
	Tip Chord	0.41 in.
	Max Root Chord	1.15 in.
	Min Root Chord	0.62 in.

There is mention of an Optimum AOA, which increases the lift to drag ratio of the UAV. This allows for the maximum lift of an airplane wing during take-off. (Kramer, 1932) states that one of the causes of the increase of lift is the increase of wind speed. This is beneficial for the UAV to quickly gain altitude when the environment is limited in range. However, because the increase in wind speed increases an aircraft's lift, this is also true for drag (Figure 3.6).

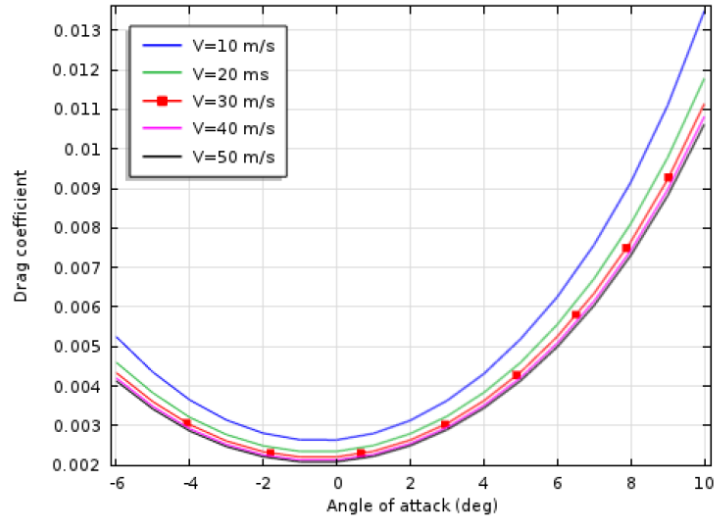


Figure 3.6: AOA vs Drag Coefficient (Sogukpinar & Bozkurt, 2015)

This is why the Optimum AOA is the best lift to drag ratio, producing the maximum amount of lift with the minimum amount of drag. It is shown that the lift to drag ratio increases in proportion to the wind speed (Sogukpinar & Bozkurt, 2015). Studies have also proven that for all speeds, the maximum lift to drag ratio was reached at the same AOA (Figure 3.7). Figure 3.7 shows the Optimum AOA to be at about  $4^\circ$  for that specific UAV (Sogukpinar & Bozkurt, 2015). This value will vary between Airfoil type, the surface area of the wing, the drone's weight etc. From the calculations that have done for the Albatross UAV, it was discovered that the Optimum AOA for this simulated UAV is at  $4.5^\circ$  (Figure 3.8). This was done by setting a velocity value, calculating the lift, and the drag at every available AOA from the wing profile, then solving for the highest lift to drag ratio. Only one velocity value was used because again, the previous study showed that for all speeds, the Optimum AOA was reached at the same value.

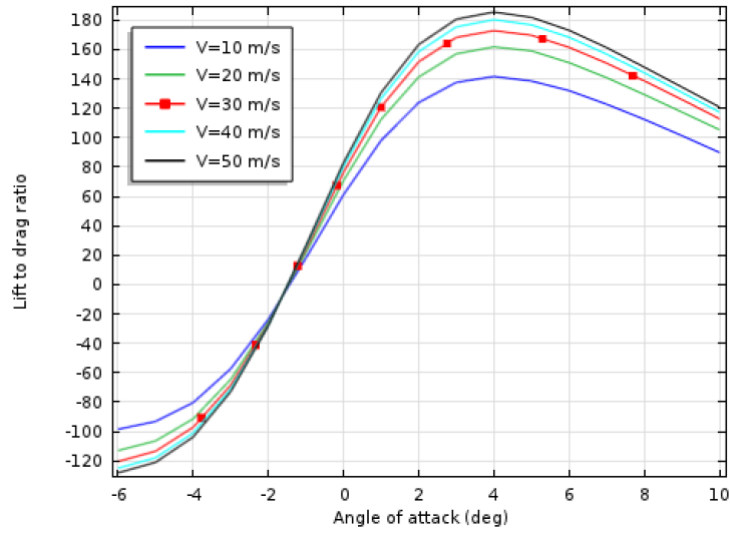


Figure 3.7: AOA vs Lift to Drag Ratio (Sogukpinar & Bozkurt, 2015)

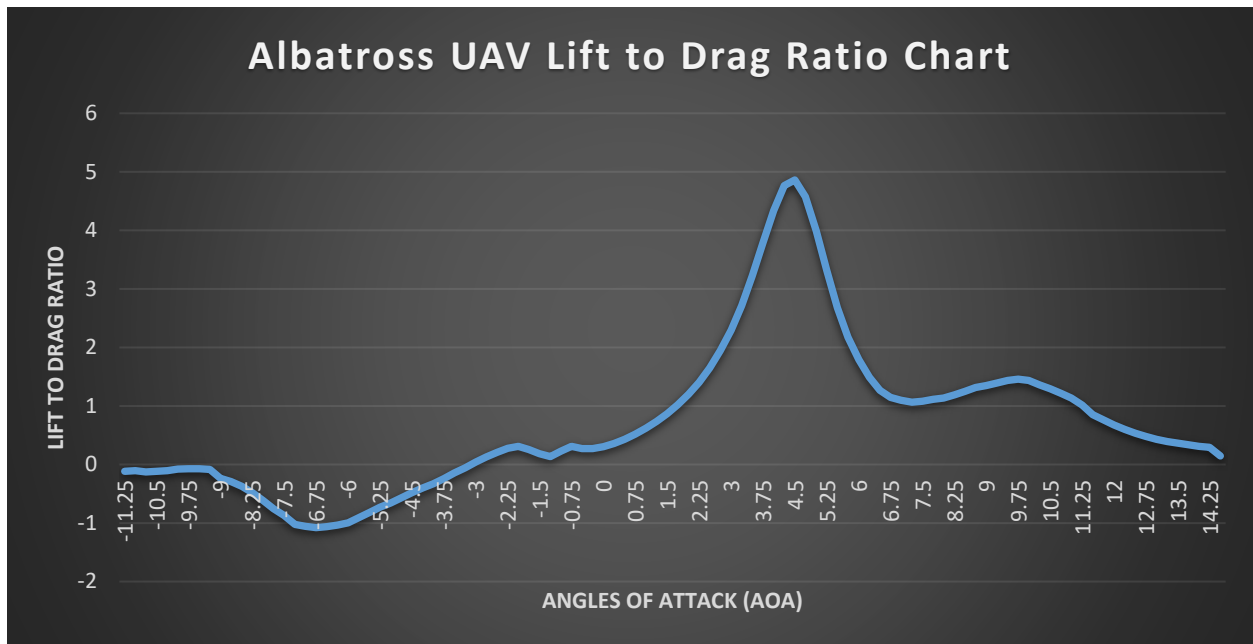


Figure 3.8: Albatross UAV Lift to Drag Ratio

### 3.4 FIXED-WING TO HOVER STUDY

The transition from FW flight to hover was further investigated as well. These transitions are mostly studied in tail-sitter, tilt-rotor, and tilt-wing UAVs because, unlike the Quadplane, the rotors of these UAVs can be used in a larger rotation of motion ranging from at least  $0^\circ$  to  $90^\circ$ . Hover and deep stall maneuvers have been used for a tail-sitter UAV to be able to perch the UAV up against the wall of a building (Marchini, 2013)(Figure 3.9).



Figure 3.9: Perching Tail-Sitter UAV (Marchini, 2013)

Another back-transition method from a Quadplane study does not angle the UAV to transition from FW flight to hover. Instead, a negative amount of thrust is applied on the pusher rotor (Figure 3.10) to assist in slowing the UAV from FW flight (Govdel, Muzaffae, Raj, Elhadidi, & Kayacan, 2019). While the quadrotor decelerates from the forward moving direction; this allows for the hover rotors to start producing thrust.

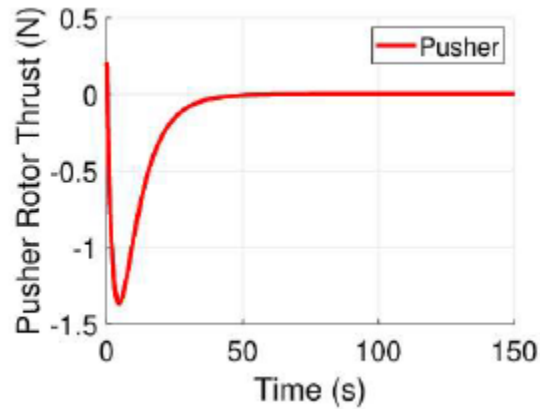


Figure 3.10: Quadplane vs. Tilt-Rotor Pitch Angle Comparison (Govdel, Muzaffae, Raj, Elhadidi, & Kayacan, 2019).

### 3.5 STALL

A stall can occur in the middle of flight, not just during a UAV take-off or transitions. There are many different types of stalls, but the main ones focused on to be sure to avoid with the types of transitions focused in this study were the following (Basson, 2010):

**Power-on stalls:** Power-on stalls will occur at take-off when straight climbs are occurring. With the nose of the aircraft rising and the climb in attitude, this may result in an accidental stall. This can occur during the transition for hover to FW flight when pitching the Quadplane back to produce the maximum amount of lift possible.

**Secondary stalls:** Secondary stalls occur when recovering from a preceding stall. Since the hover rotors were shut off at a high altitude to produce a nose-dive or straight downward projection, it is essentially causing an initial stall, and then recovering from it to produce the transition.

Spin: Spin tends to result in autorotation. Again, with shutting off the hover rotors at a high altitude to begin a downward projection of the Quadplane; spin could occur when the outside wing is less stalled than the inside wing, causing a downward rolling, pitching, and yawing spiral.

## Chapter 4: Methodology

### 4.1 Calculations

This study was first approached by seeing what calculations were needed to take place to simulate the dynamic transition for the Quadplane within MATLAB. The first portion was for the hover motors to provide the lift in the z-axis before the transition. This also included their direction of rotation, distance location from the COG, and detailed data about the motor and propeller selection for this specific UAV to determine the maximum amount of thrust each rotor could produce.

Once the calculations for the hover portion was completed, defining the wing of the Albatross was next. With the wing profile of the UAV and taking the AOA into consideration; Coefficients of Lift (CoL), Coefficients of Drag (CoD), Coefficients of Mass (CoM), and Center of Pressure (CoP) values determined, . That helped obtain the most accurate results for lift, drag, etc., when testing.

Some specific calculations that affected the transitions during this study were solving for the desired altitude and desired velocity. In order to not lose any altitude during each of the transitions from hover to FW flight, it was necessary to solve for the desired altitude in order to get enough error from the controller to solve for the required forces. From Equation 4.1, the total forces in the controller were solved by taking the error in the positions and multiplying them by the proportional gain values. They were then added by the error in velocities multiplied by the derivative gain values. Equation 4.2 shows solving for the desired altitude from the force in the z-direction. It was known what force in the z-direction for the hover motors was needed, which is 22 lbs. since that is the weight of the UAV. The initial altitude and control gain values were known

as well. The final step was to then solve for the desired altitude and use that value to achieve no loss in altitude during the transitions.

$$F_{XYZ} = (\mathit{Desired}_{pos} - \mathit{Initial}_{pos}) * \mathit{Control}_P \quad \text{Eq. 4.1}$$

$$+ (\mathit{Desired}_{vel} - \mathit{Initial}_{vel}) * \mathit{Control}_D$$

$$F_Z = (\mathit{Desired}_{Alt} - \mathit{Initial}_{Alt}) * \mathit{Control}_P \quad \text{Eq. 4.2}$$

The next portion for the desired velocity required using the calculations for lift and drag force from the wing shown in Equations 4.2 and 4.3. From these equations:

$\rho$  is the density of air

SA is the surface area of the wing

CL is the coefficient of lift

CD is the coefficient of drag

V is velocity

Knowing the current velocity of the UAV during each time step, it was possible to solve for the values of lift and drag force during the transitions. This was able to give the force from the wing in the x-, y-, and z- direction shown in Equations 4.4 through 4.6. The force in the y-direction from Equation 4.5 shows a value of zero because these simulations were only done in the forward moving direction. Due to the change in AOA from the different transitions done, the desired velocities for each transition were needing to change as well. To solve for each of the desired velocities used during the simulations, it was very similar to solving for the desired altitude, but

this time, the force in the z-direction from the wings was used (Equation 4.6). Again, it was known that 22 lbs. of force in the z-direction was needed to not lose any altitude during the transitions or flight, and because lift and drag force are both dependant on velocity, solving for velocity is what was used for the desired velocity in the controller.

$$Lift = \frac{\rho * SA * CL * V^2}{2 * 32.2} \quad \text{Eq. 4.2}$$

$$Drag = \frac{\rho * SA * CD * V^2}{2 * 32.2} \quad \text{Eq. 4.3}$$

$$F_x = -lift * sin(AOA) - drag * cos(AOA) \quad \text{Eq. 4.4}$$

$$F_y = 0 \quad \text{Eq. 4.5}$$

$$F_z = -lift * cos(AOA) + drag * sin(AOA) \quad \text{Eq. 4.6}$$

#### 4.1.1 Coordinate Systems

Coordinate systems were studied for this project to determine the frames in which the results were needed to be. They would either be inertial, also known as the world-coordinate system, or body-fixed frame (Diebel, 2006). The inertial frame is an Earth-fixed set of axes where the x-axis is pointing North, the y-axis is pointing East, and the z-axis points downward towards the center of the Earth (Figure 4.1). Because the z-axis point downward, any height above ground

is considered to be a negative value. The body frame is a coordinate system on the aircraft where the x-axis points out the UAV's nose. The y-axis points out the right-wing, and the z-axis points out the bottom of the fuselage (Figure 4.2).

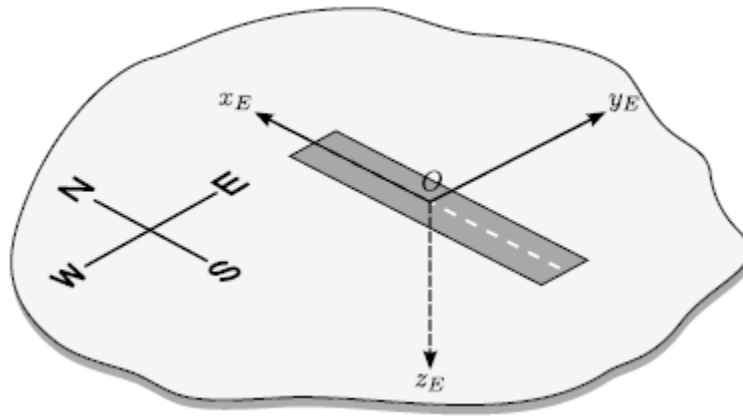


Figure 4.1: Inertial Reference Frame (Basson, 2010)

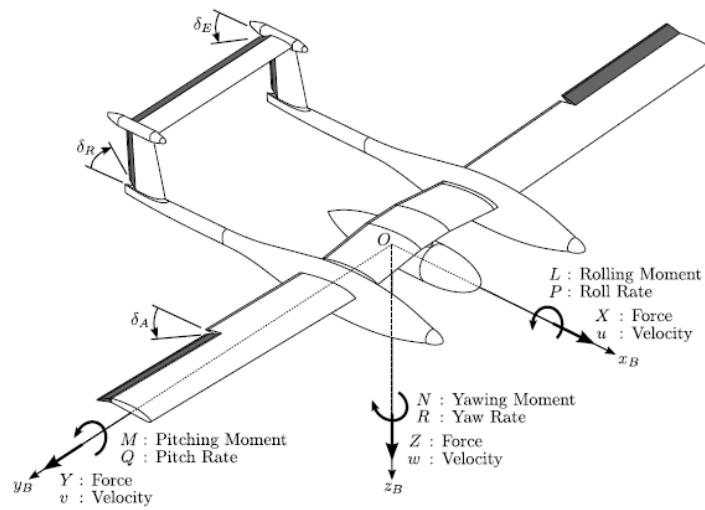


Figure 4.2: Body Reference Frame (Basson, 2010)

For the Albatross UAV, some multiple forces and torques that are not all in the same frame (Figure 4.3). Gravity is not fixed to the UAV; therefore, the drone's weight is initially in the inertial reference frame. All of the thrusts have been applied on the UAV, both for hover and FW flight, are in the body reference frame. With the forward-moving thrust, drag force and lift force occur, and these forces are also in the body frame. The forces being applied to the UAV also cause torque to occur in the body frame.

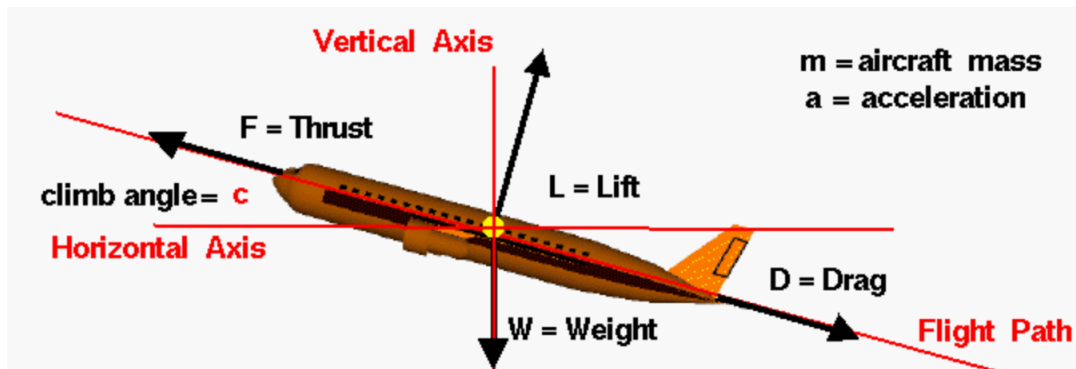


Figure 4.3: Forces on an Aircraft (Forces in a Climb, n.d.)

Even though most of the forces occur in the body reference frame, every single force needs to be in the same frame. It is impossible to apply the force values together in the simulation, with them being in different reference frames. To switch the forces from inertial to body frame or vice versa; they need to apply rotation matrices about single rotation coordinate axes, such as the roll around the x-axis, pitch around the y-axis, and yaw around the z-axis were used (Equations 4.1 through 4.3). This allowed us to simulate and show the results in the inertial reference frame since this is a UAV and made it easier to reference the forces, velocities, and positions.

$$R_x = \begin{bmatrix} 1 & 0 & 0 \\ 0 & \cos \theta & -\sin \theta \\ 0 & \sin \theta & \cos \theta \end{bmatrix} \quad \text{Eq. 4.7}$$

$$R_y = \begin{bmatrix} \cos \theta & 0 & \sin \theta \\ 0 & 1 & 0 \\ -\sin \theta & 0 & \cos \theta \end{bmatrix} \quad \text{Eq. 4.8}$$

$$R_z = \begin{bmatrix} \cos \theta & -\sin \theta & 0 \\ \sin \theta & \cos \theta & 0 \\ 0 & 0 & 1 \end{bmatrix} \quad \text{Eq. 4.9}$$

## 4.2 Algorithm

The next step was the MATLAB algorithm. At the beginning of the code is when the input all of the parameters and information for the motors, propellers, and the wings along with the weight of the UAV, its moments of inertias, and air density. Then begins stating the initial and desired conditions that get called into the PD controller to solve for the forces and torques from the rotors. That then determines the UAV's velocity that gets used to solve the lift and drag being produced by the wing and solving for the forces and torques from there. The total amount of forces determined, and torque was solved for at that time step and then loops all over again with those new values until the errors of what we want become 0.

## 4.3 Testing

During the testing, data were plotted to see the results in the desired periods. From the plots, one will show how much force is being produced from each of the five rotors based on the initial and desired conditions. Once the desired speed in the forward-moving direction was reached to create enough lift for the UAV, the FW flight rotor would fully take over, and thrust in all the

hover rotors are no longer needed. There would only be thrust in motors two and three, which are on the left-hand side of the UAV; to counteract the torque produced from the FW flight rotor along the negative x-axis during the transition. Another plot defines the velocities in the inertial frame produced in the x-, y-, and z-axes. Defined from the Dronecode flight control software, the transition was fully completed once the UAV achieved its desired velocity. Like the velocities; the inertial position is also plotted in the x-, y-, and z-axes to show how far and in what direction the UAV has traveled. This plot will also show the amount of distance traveled in the x-direction when the transition is completed, as well as the altitude gain/loss during the transition.

The testing and simulations were all done through MATLAB due to time constraints. To ensure this methodology closely matched transitions of other flight controllers, following the Quadplane VTOL Configuration & Tuning through the Dronecode flight control software was done.

## Chapter 5: Results and Discussion

### 5.1 HOVER TO FIXED-WING TRANSITIONS

#### 5.1.1 Baseline Transition (No Altitude Loss)

The baseline transition from hover to fixed-wing flight is done from starting up the FW rotor while the Albatross UAV is in hover mode. For this flat-level transition, the UAV's initial conditions will start at 65.6 feet in altitude, 0 ft/sec forward moving velocity, and pitched at  $0^\circ$ . The desired conditions were to increase the altitude to 67.8 feet, so there is no loss in altitude during the transition, reaching 54.8 ft/sec for the forward moving velocity and remaining at a pitch angle of  $0^\circ$ , which provide an AOA of  $7^\circ$ . The wings are already angled back by  $7^\circ$  when level-UAV is there.

Because these simulations were more focused on reaching desired x-velocities, the proportional control error values for the x-position remained at 0, while the derivative value for the x-velocity used was 10. Because all the transitions were only done in a forward moving velocity, the proportional and derivative control error values for y-position and y-velocity remained at 0. The proportional and derivative values for z-position and z-velocity were both at values of -10, because any altitude above ground is a negative value in the z-direction. This value was not 0 because there were still desired altitude values that were wanting to be reached.

Figure 5.1 shows the forces for the baseline transition. Columns 1 through 4 represent the hover rotors' forces, and column 5 represents the force for the FW rotor. The FW rotor begins with its maximum amount of force since the x-velocity error is so great at the start of the simulation. The four hover rotors remain active at 5.5 lbs. each for a short time shows that it is hovering. As the FW rotor is starting up when there changes in the forces from the hover rotors. The controls in hover mode start to decrease, and FW mode is increasing to where it begins to produce enough

lift in the negative z-direction to where the hover rotors are no longer needed. You can also see a dip in the force for the FW rotor. The reason for this is because the UAV is reaching its desired velocity and begins to stabilize at that time.

As you can see, hover rotors 2 and 3 show more thrust than rotors 1 and 4 during the transition. As stated in Figure 3.1, rotors 2 and 3 are located on the left side of the UAV. The reason these two rotors are producing a greater amount of force is to counteract the torque that is being produced from the FW rotor during the transition; similar to what happens to a helicopter. The torque causes a slight counterclockwise rotation of the UAV about the x-axis, and rotors 2 and 3 are what is keeping the UAV stabilized. Once the UAV has achieved FW flight, the autopilot from the Dronecode flight control software keeps the UAV stabilized.

Figure 5.2 shows the velocities for the UAV in the x-, y-, and z-direction. There is a slight overshoot for the x-velocity shown in blue. The reason the UAV overshoot is that the error was so great at the beginning of the simulation that the controller wants the UAV to get up to speed, then it overshoot, and so that's when the force in the FW rotor holds back from its maximum value to slow down and begins to slowly pick back up again to maintain a velocity closest to the desired x-velocity. According to the Dronecode flight control software, the transition is completed, and the UAV has fully obtained flight once the desired velocity has been reached. For this transition, the UAV has fully obtained flight at about 7.4 sec. The red shows a velocity in the y-direction which remains at 0 ft/sec. The yellow is the velocity in the z-direction, which you can see increases and decreases slowly as the transition occurs before stabilizing at 0 ft/sec.

The positions of the UAV are shown in Figure 5.3. In red shows the increase in altitude in the negative z-direction while the UAV was transitioning. At the beginning of the transition, the UAV starts at 65.6 feet in altitude. As the hover controls are decreasing and the FW controls are

increasing, as well as the velocity in the x-direction, the altitude gain overshoot to a value of 68.14 feet before stabilizing at 67.8 feet. There was no loss in altitude during this transition. The UAV traveled about 195.5 feet in the x- direction until the transition was completed and 0 feet in the y-direction.

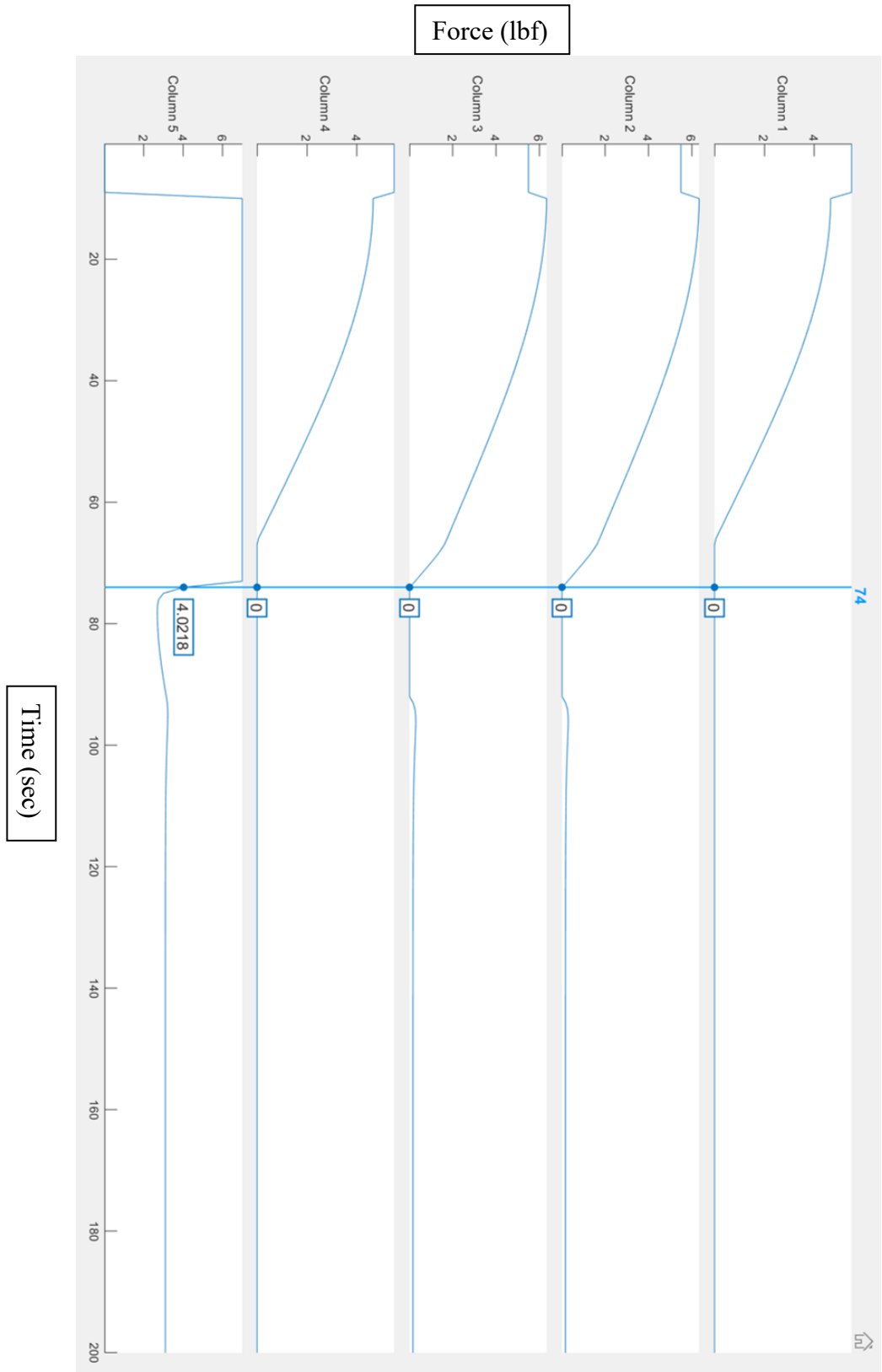


Figure 5.1: Baseline Transition Forces

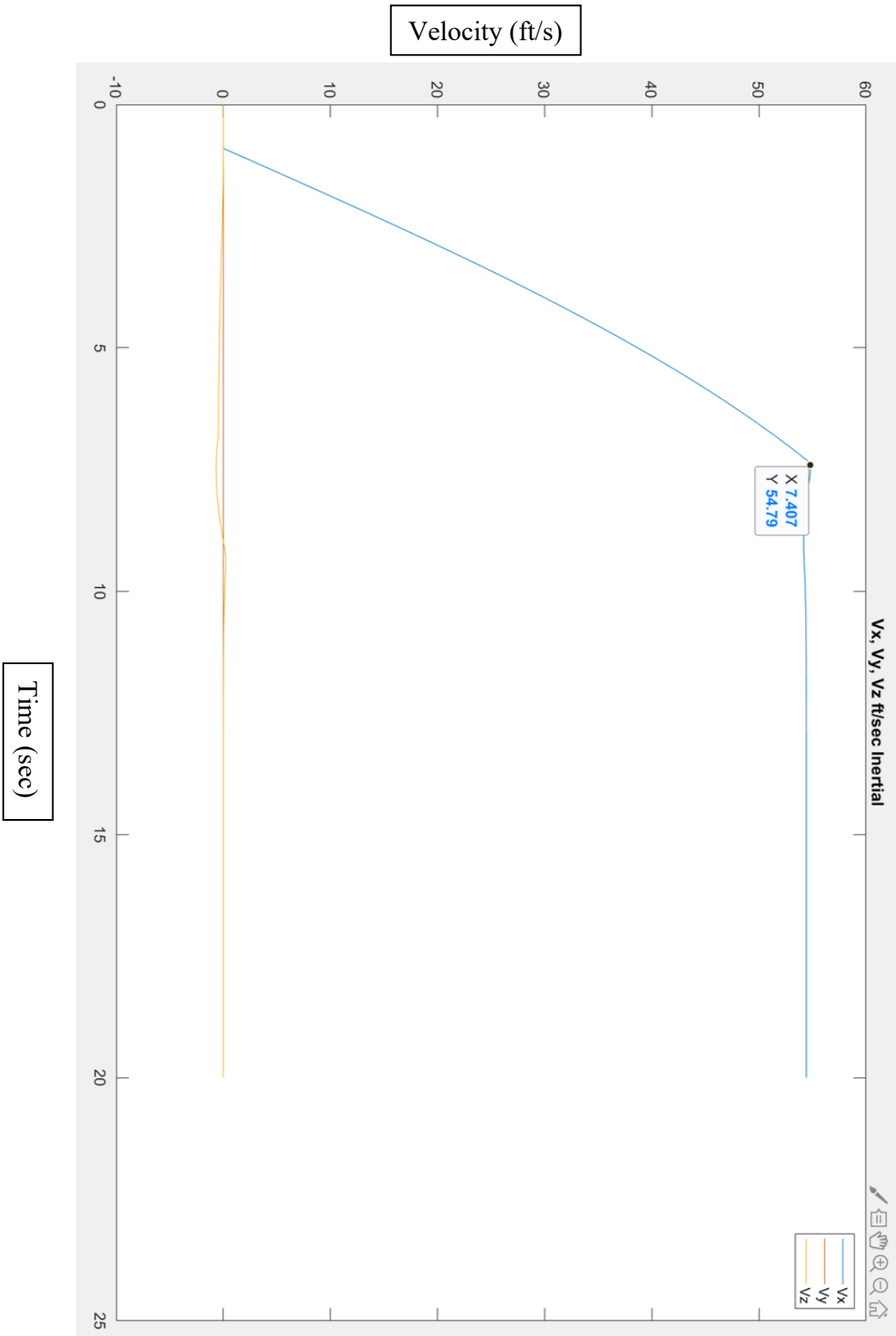


Figure 5.2: Baseline Transition Velocities

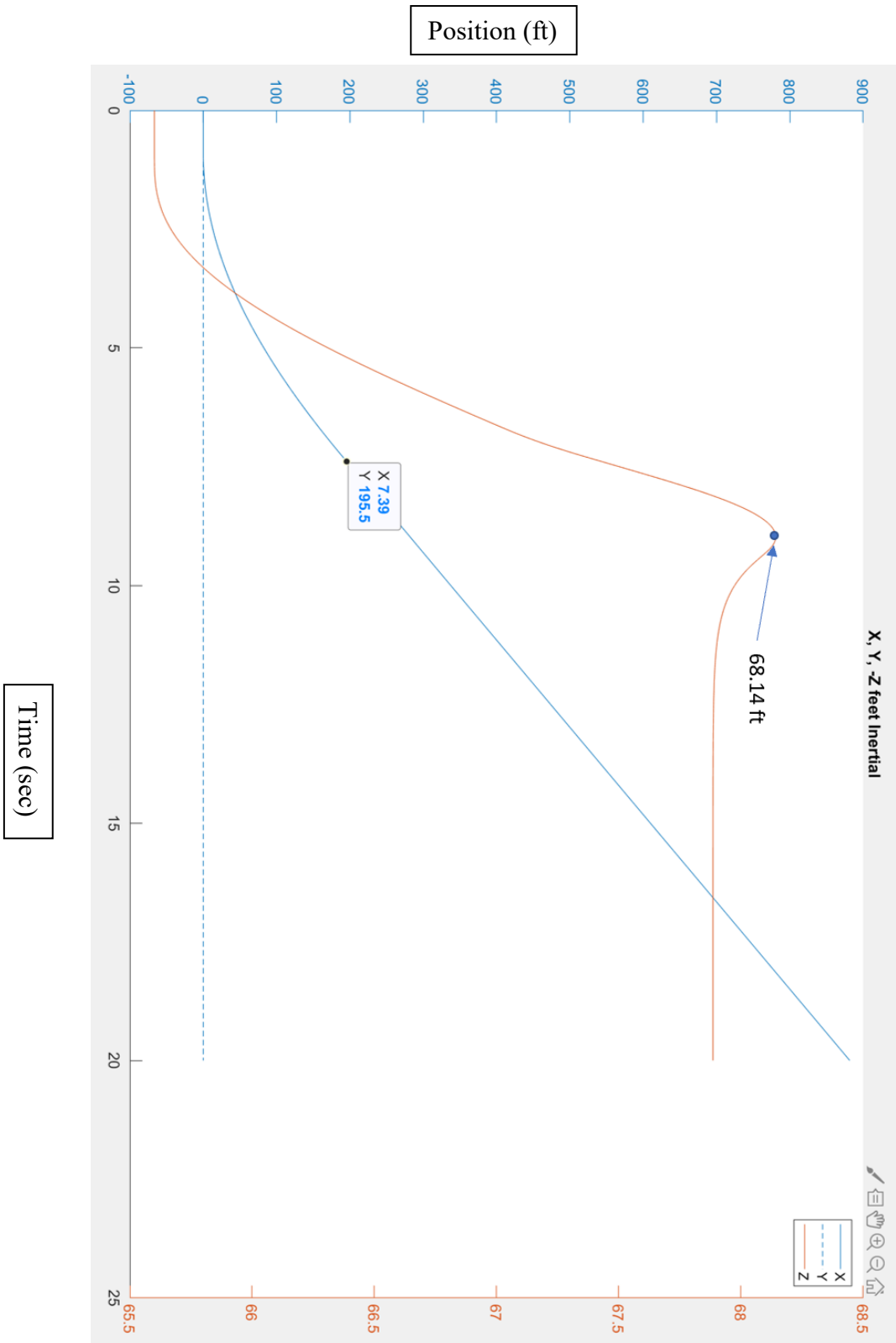


Figure 5.3: Baseline Transition Positions

### 5.1.2 Flat Level Transition (Same Initial/Desired Altitude)

This next hover to fixed-wing transition is very similar to the baseline transition, where the conditions are the same except for the desired altitude. The initial velocity is 0 ft/sec, the desired velocity is 54.8 ft/sec, and the initial and desired pitch were to remain at  $0^\circ$ . The initial altitude and desired altitude for this transition were the same at 65.6 feet. The control error values were the same as the previous transition.

Figure 5.4 shows the forces for this flat level transition. They seem very similar to the previous forces shown for the baseline transition, but the difference is that the forces for this transition show an increase in the forces for each of the hover rotors shown in columns 1 through 4 for a short time. This happens because as the transition occurs, the control picks up that the UAV is already at the desired altitude set, which means the error from initial to the desired condition is zero. When this happens, the controller communicates to the hover rotors that because the error is zero, there is no longer a force needed to be required by the hover rotors. They stop producing thrust for a short amount of time and cause the UAV to lose altitude. In the very first time step of Figure 5.4, the hover rotors are beginning to produce thrust again because there is now a nonzero error value in the altitude.

Showing the velocities in Figure 5.5, again, they look very similar to the previous transition velocities. This plot even shows the UAV fully transitioning at the same length of time at 7.4 sec, but what has changed was the velocity in the z- direction. This time the velocity begins the slow increase in the negative z-velocity before stabilizing. The velocity in the y-direction remains 0 ft/sec.

The UAV positions shown in Figure 5.6 are the main portion of the simulation that showed the most change. The change in altitude for the negative z-direction is shown in red. At the

beginning of the transition, the UAV starts at 65.6 feet in altitude. The lowest altitude the UAV reaches during this transition is 63.62 feet, which was expected due to having the same initial and desired altitude conditions. The highest it reaches is 65.94 feet before stabilizing at 65.6 feet. The UAV had no change in position for the y-direction and traveled about 195.7 feet in the x-direction until the transition was completed.

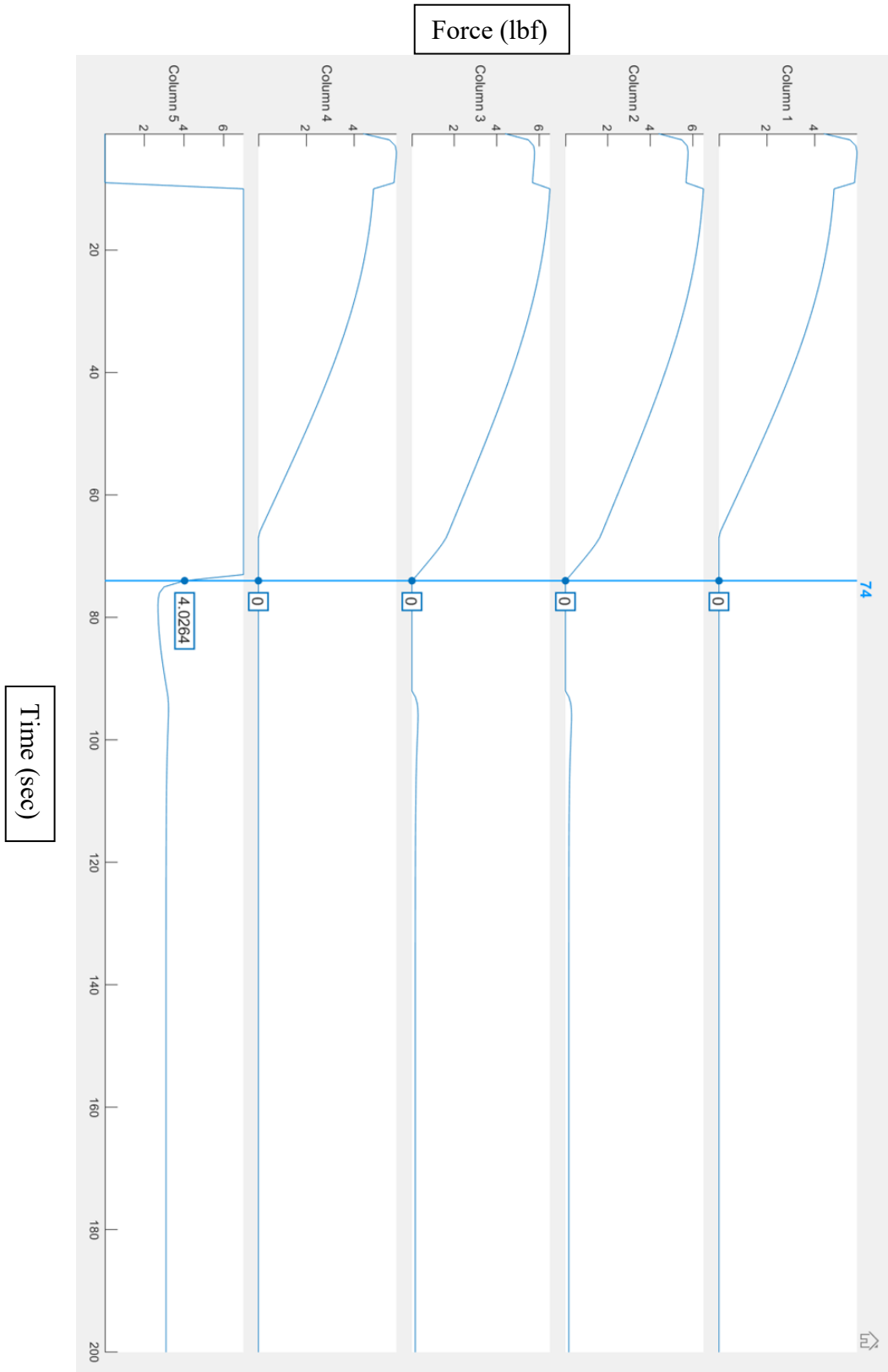


Figure 5.4: Flat Level Transition Forces

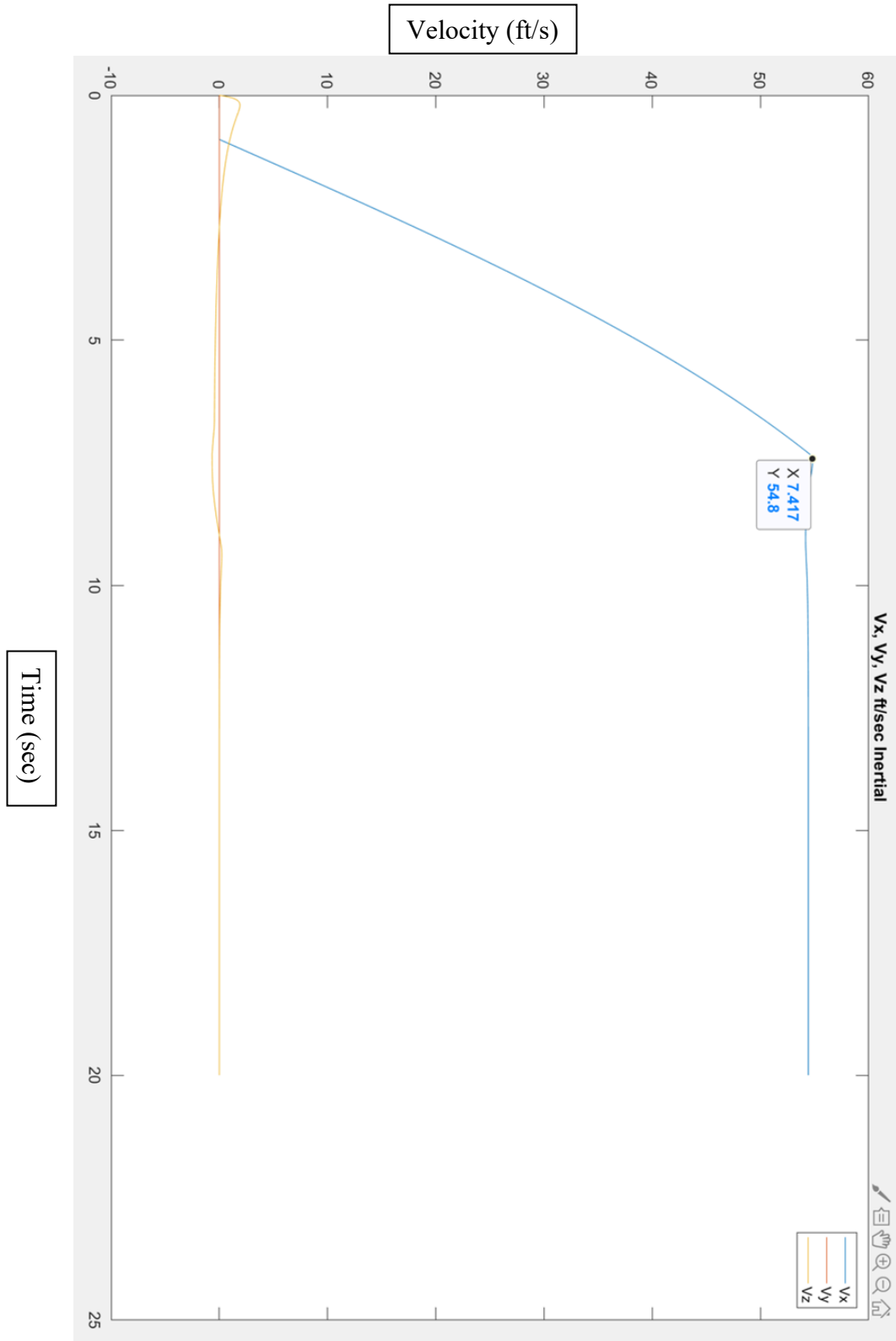


Figure 5.5: Flat Level Transition Velocities

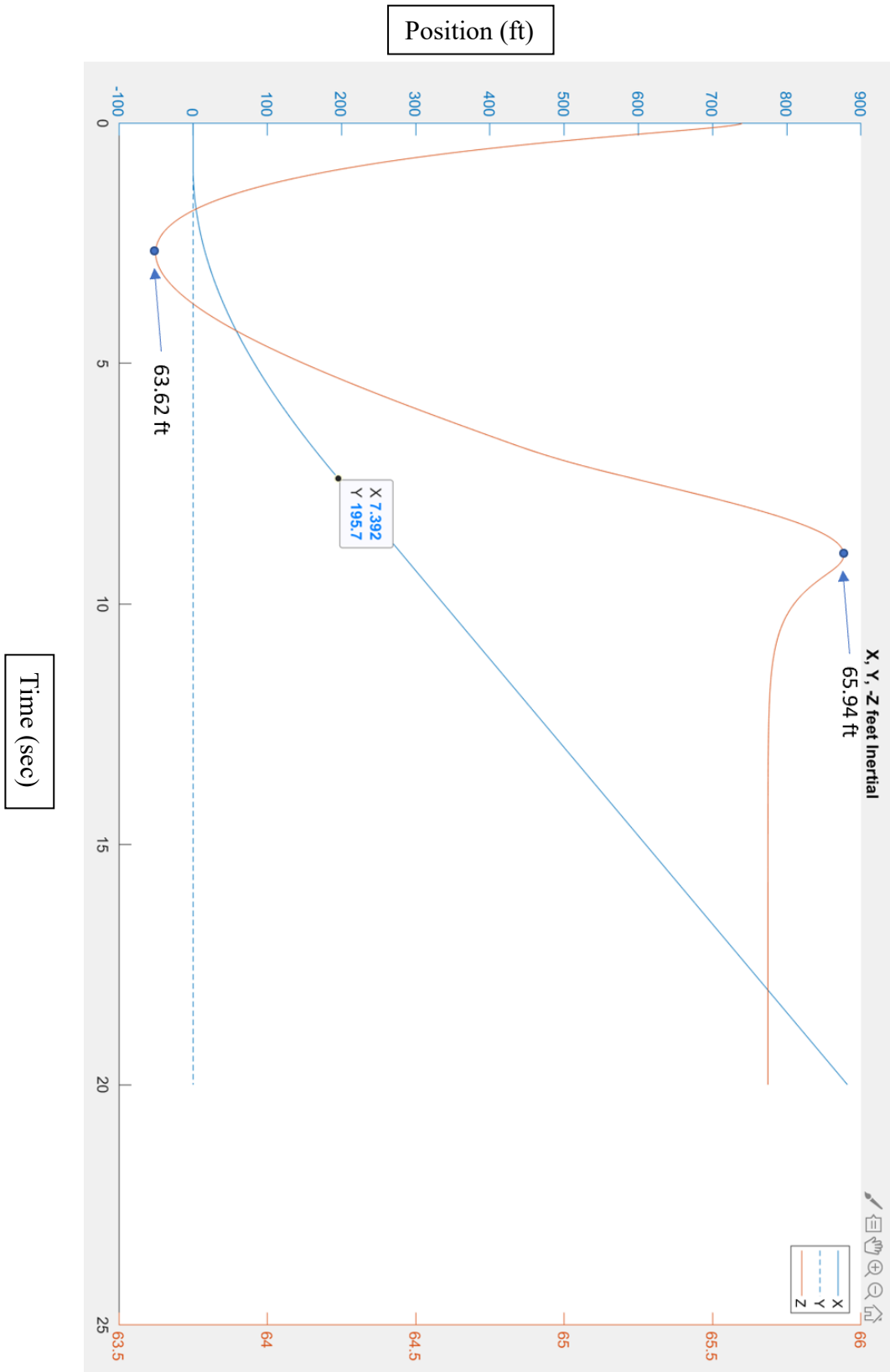


Figure 5.6: Flat Level Transition Positions

### 5.1.3 Pitched-Back Transition (No Altitude Loss)

For the pitched-back transition, the UAV began with the same initial conditions of hovering at 65.6 feet in altitude, 0 ft/sec in the forward-moving velocity, and a pitch of  $0^\circ$ . The desired conditions were to have it reaching an altitude of 67.8 feet. So there would be no loss in altitude during the transition, reaching a forward-moving velocity of 48.2 ft/sec, and transition at a pitched angled of  $4^\circ$ , provided an AOA of  $11^\circ$ , which is right below the critical AOA. For this transition, the desired velocity was able to be decreased because of the higher AOA. The control error values remained the same.

The pitched-back transition forces in Figure 5.7 start off very similar, which is expected since the transitions are all starting off with the same initial conditions. As the velocity in the UAV is increasing, the forces in rotors 1 through 4 are decreasing, and FW mode is beginning to take over. The forces in motors 2 and 3 are also producing more thrust than rotors 1 and 4 to stabilize the Albatross during the transition.

As the Albatross is increasing in velocity in the x-direction during the pitched-back transition shown in Figure 5.8, the UAV fully obtains flight when reaching its desired velocity at 7.81 sec. The red shows a velocity in the y-direction which remains at 0 ft/sec. The yellow is the velocity in the z-direction, which you can see slowly increases and decreases as the transition is occurring.

The positions for the pitched-back transition are shown in Figure 5.9. For this transition, there was no overshoot in altitude and stabilized at 67.8 feet. The position in the y-direction remained at 0 feet, and the UAV traveled 199.3 feet in the x-direction before the transition was fully completed.

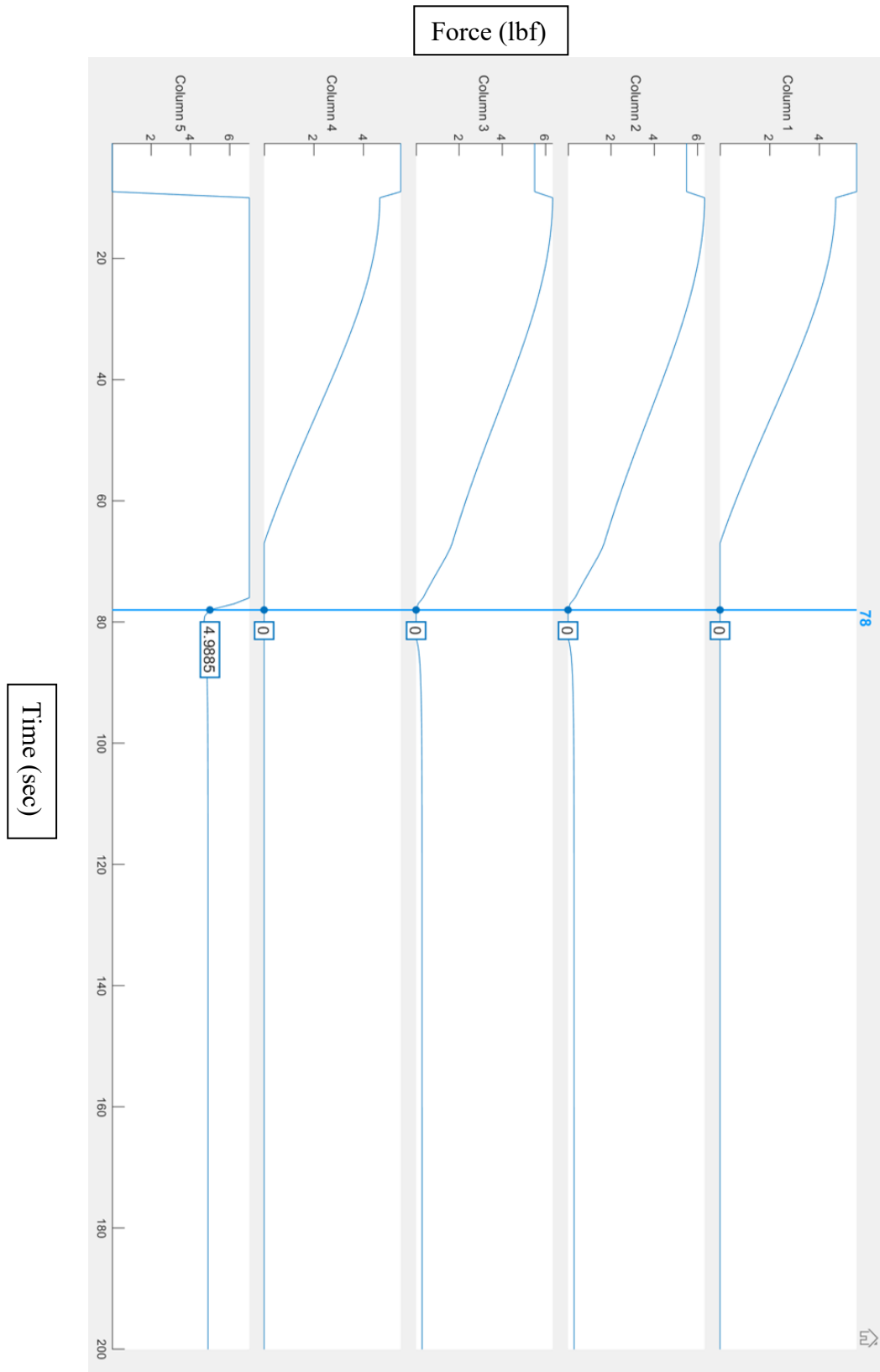


Figure 5.7: Pitched-Back Transition Forces

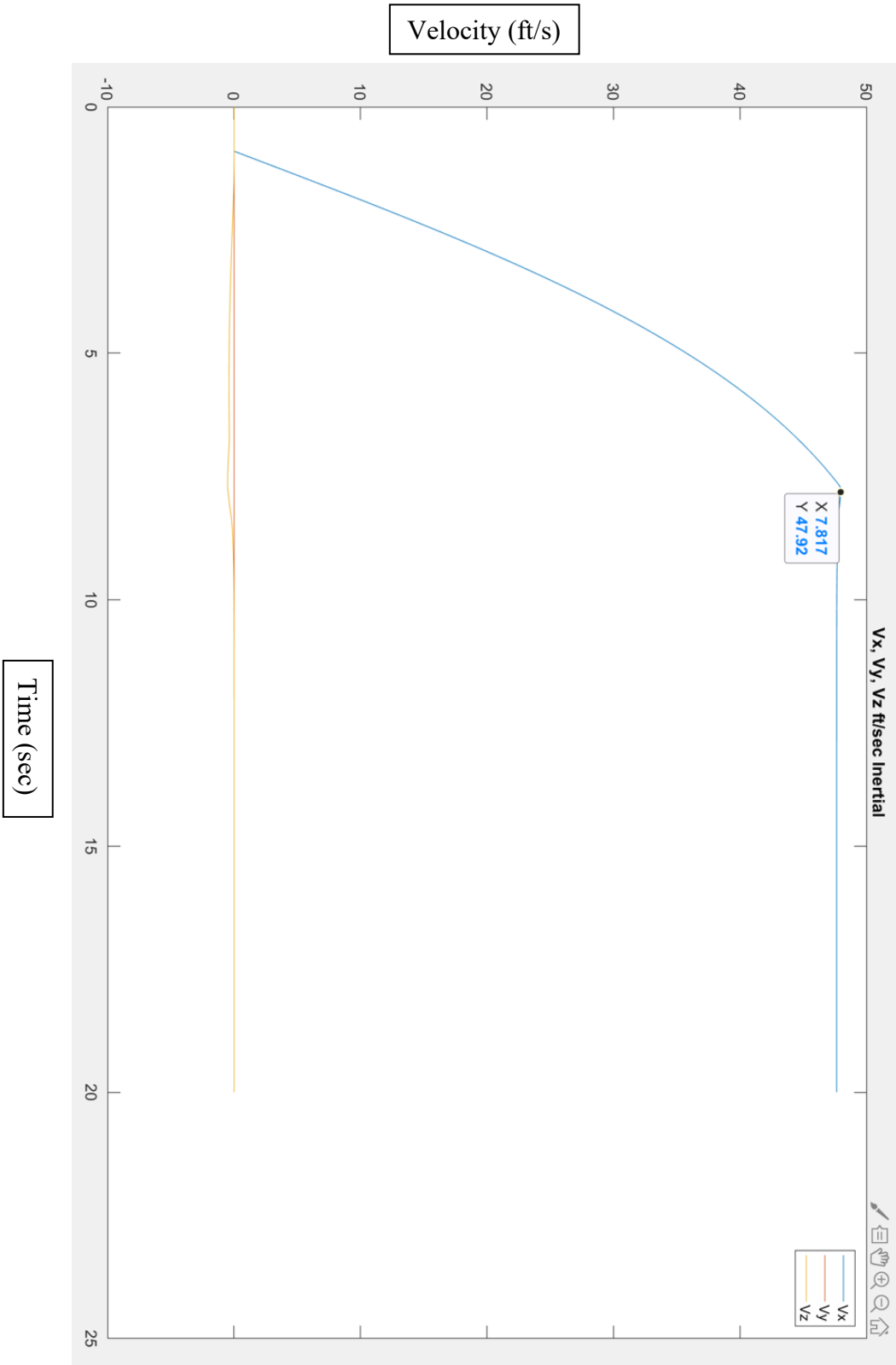


Figure 5.8: Pitched-Back Transition Velocities

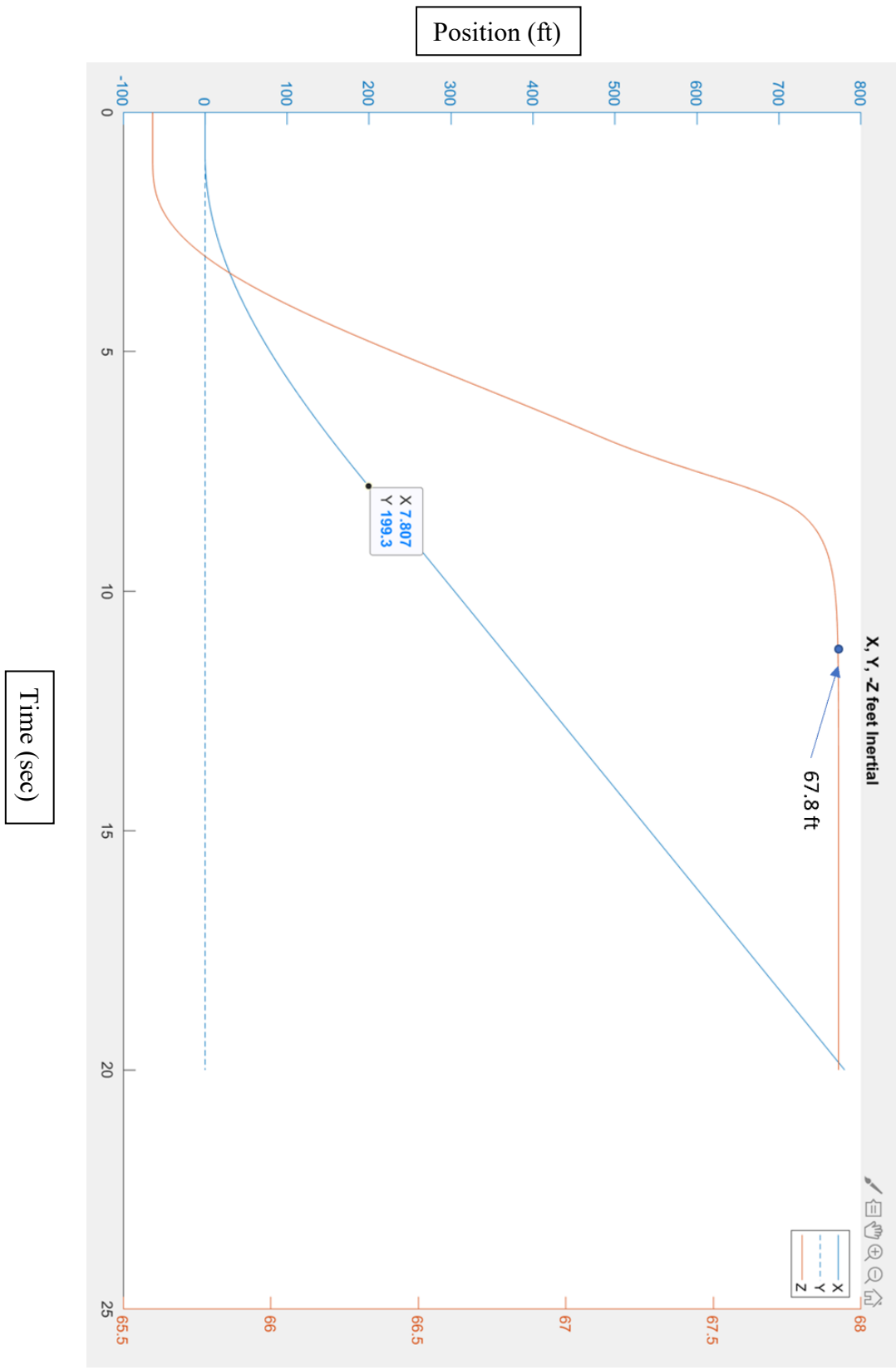


Figure 5.9: Pitched-Back Transition Positions

#### 5.1.4 Pitch-Forward Transition (No Altitude Loss)

The fourth transition simulated was the pitched-forward transition. For this transition, the Albatross UAV was pitched forward by  $-2.5^\circ$ , causing the wing's AOA to go from the original  $7^\circ$  to  $4.5^\circ$ . This specific angle is the Optimum AOA of the UAV to produce the best lift to drag ratio. The initial conditions were left at 65.6 feet in altitude and 0 ft/s in the forward-moving velocity, and the desired conditions were to reach an increase of 67.8 feet in elevation with a forward-moving velocity of 61.7 ft/sec. The control error values remained the same.

The forces of the UAV in Figure 5.10 for the pitched-forward transition show similar results, where as the velocity of the UAV is increasing and creating lift, the forces in the hover motors are decreasing and no longer in use once the UAV fully obtains flight. Figure 5.11 shows the x-velocity in blue for the pitched-forward transition where the Albatross fully obtains flight at roughly 7.67 sec. The y-velocity in red remains at a value of 0 ft/sec, and a slight increase and then decrease in the z-velocity is shown again before stabilizing at 0 ft/sec. The positions for the pitched-forward transition are shown in Figure 5.12 where the position in the negative z-direction overshoot by a bit more this time to 68.35 feet before stabilizing to 67.8 ft. The position in the y-direction remained at 0 feet, and once the Albatross has fully transitioned and obtained flight, it has traveled about 222 feet in the x-direction.

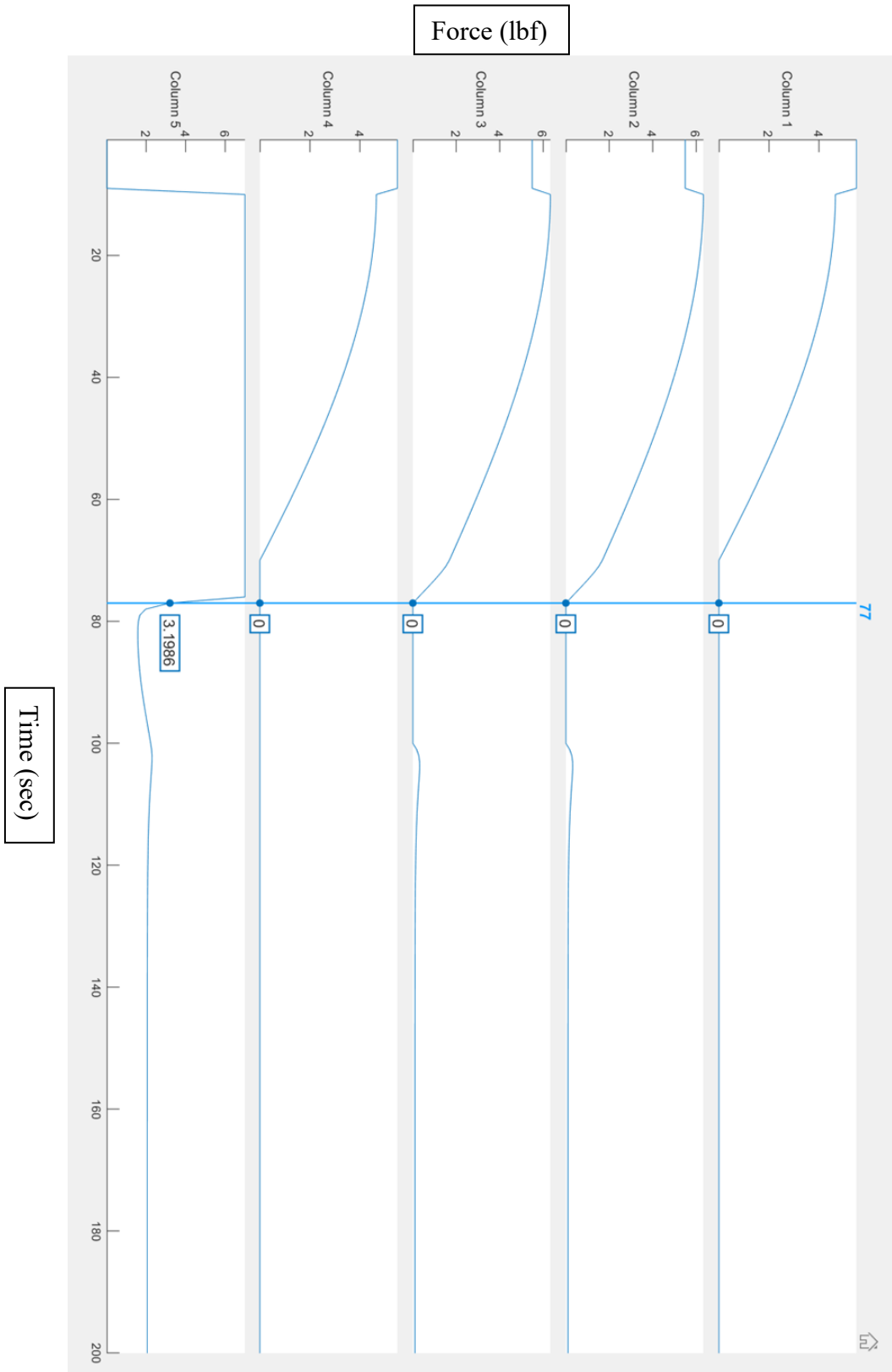


Figure 5.10: Pitched-Forward Transition Forces

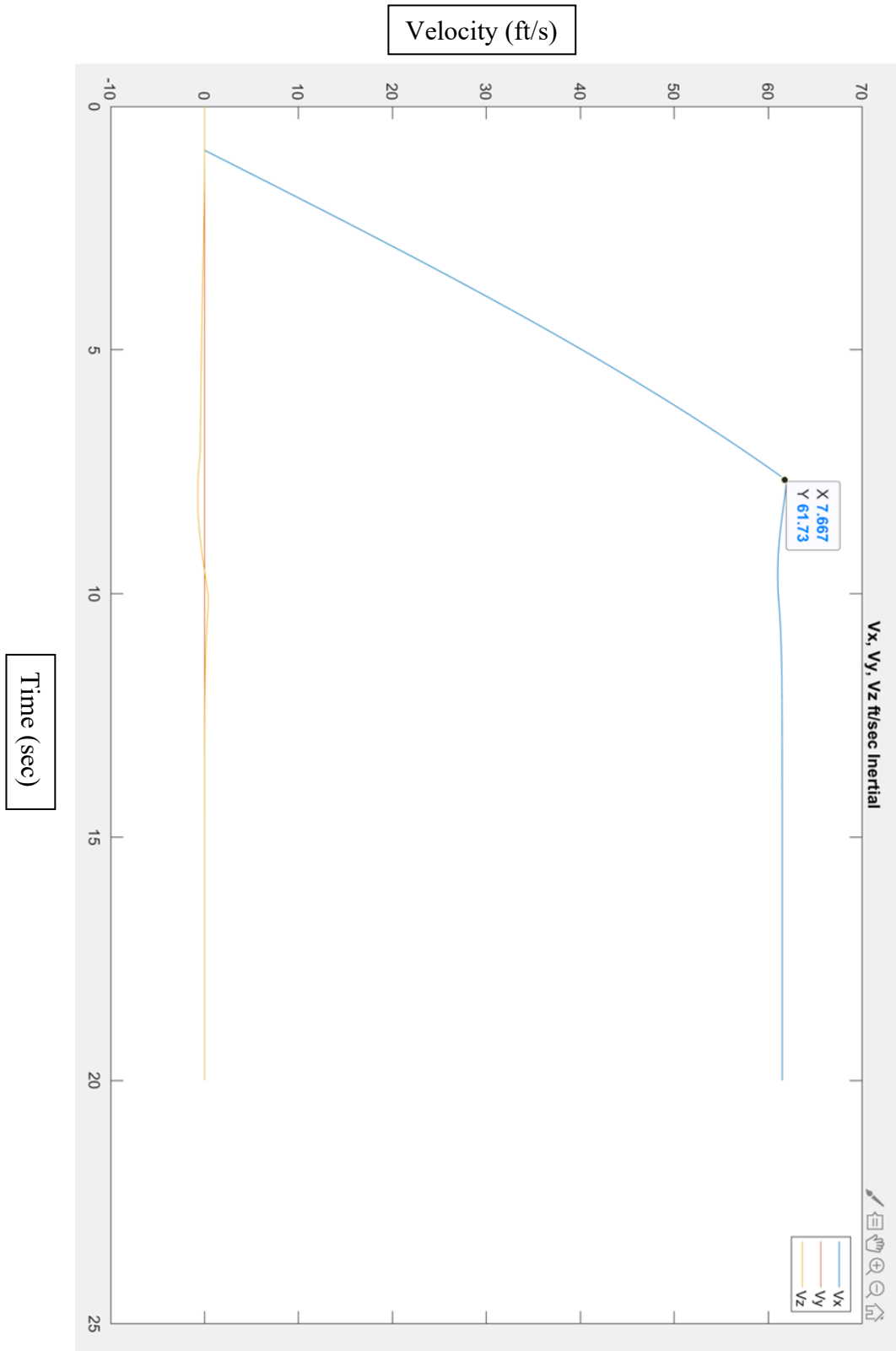


Figure 5.11: Pitched-Forward Transition Velocities

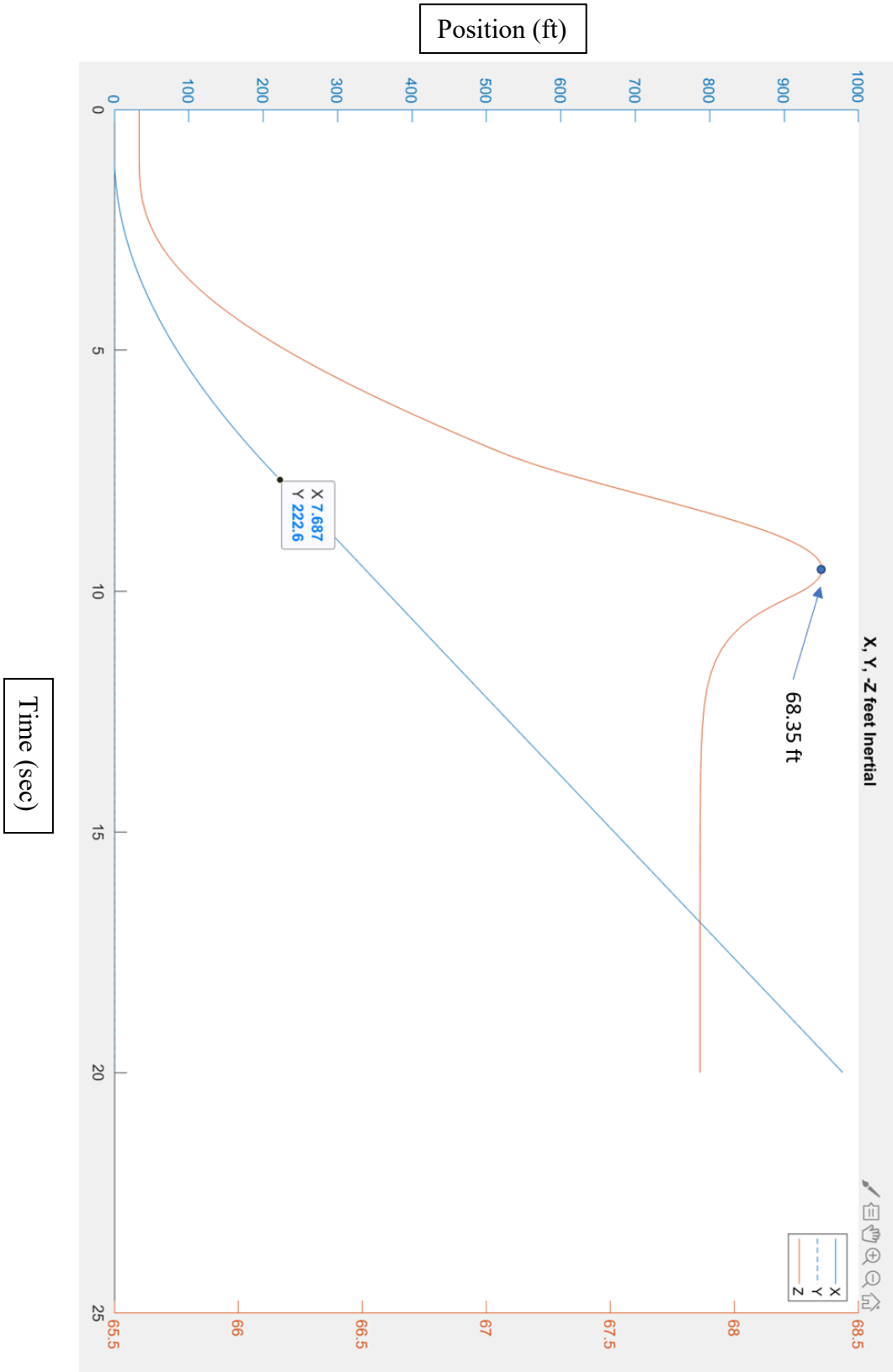


Figure 5.12: Pitched-Forward Transition Positions

### 5.1.5 Flat Free-Fall Transition (Decrease in Altitude)

For the flat free-fall transition, this is where the initial conditions change prior to the previous transitions from hover to FW flight. To better demonstrate the height limits for this transition, the conditions were changed. This transition had initial conditions of 65.6 feet in altitude, 0 ft/sec in the forward velocity, and a pitch angle of  $0^\circ$ , giving us an Angle of Attack (AOA) of  $7^\circ$ . The desired conditions were now 5 feet in altitude, 54.8 ft/sec in the forward-moving velocity, and remain at a pitch angle of  $0^\circ$ . The control error values remained the same.

For the forces in Figure 5.13 in this flat free-fall transition, rotors 1 through 4 start with forces of 5.5 lbs. Then quickly go to 0 lbs. to show that the hover rotors were shut off, and rotor 5 starts at the maximum amount of force. Quickly, the control picks up a torque in the x-axis, which was produced from the FW rotor, and rotors 2 and 3 start producing a force to counteract it.

Figure 5.14 shows when this transition fully obtains flight from plotting the velocities of the UAV. It was determined that the UAV reached closest to the desired velocity and fully obtained flight at about 7.6 sec. The y-velocity in red remains at a value of 0 ft/sec. There is a spike in the z-velocity shown as if it is free-falling before there is enough lift being produced by the wing and stabilizes at 0 ft/sec.

For the positions of the UAV in Figure 5.15 during the flat free-fall transition, you can see that in the z-position, it starts at 65.6 feet of elevation and drops down to 3.42 feet before it begins to stabilize at 5 feet in elevation. The position in the y-direction continues to remain at 0 feet throughout the simulation, and the position of the Albatross had traveled about 199 feet in the x-direction until the transition was completed.

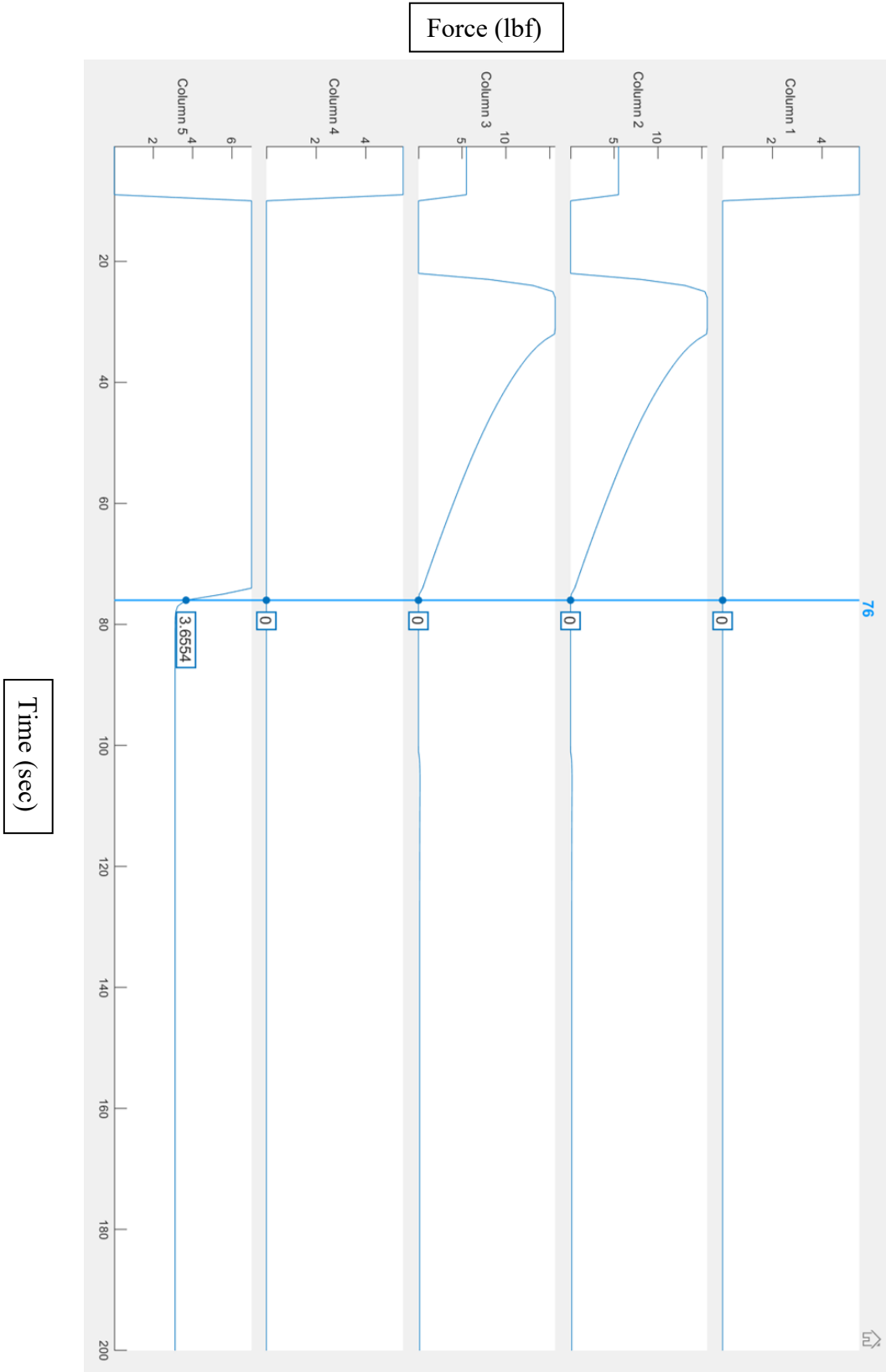


Figure 5.13: Flat Free-Fall Transition Forces

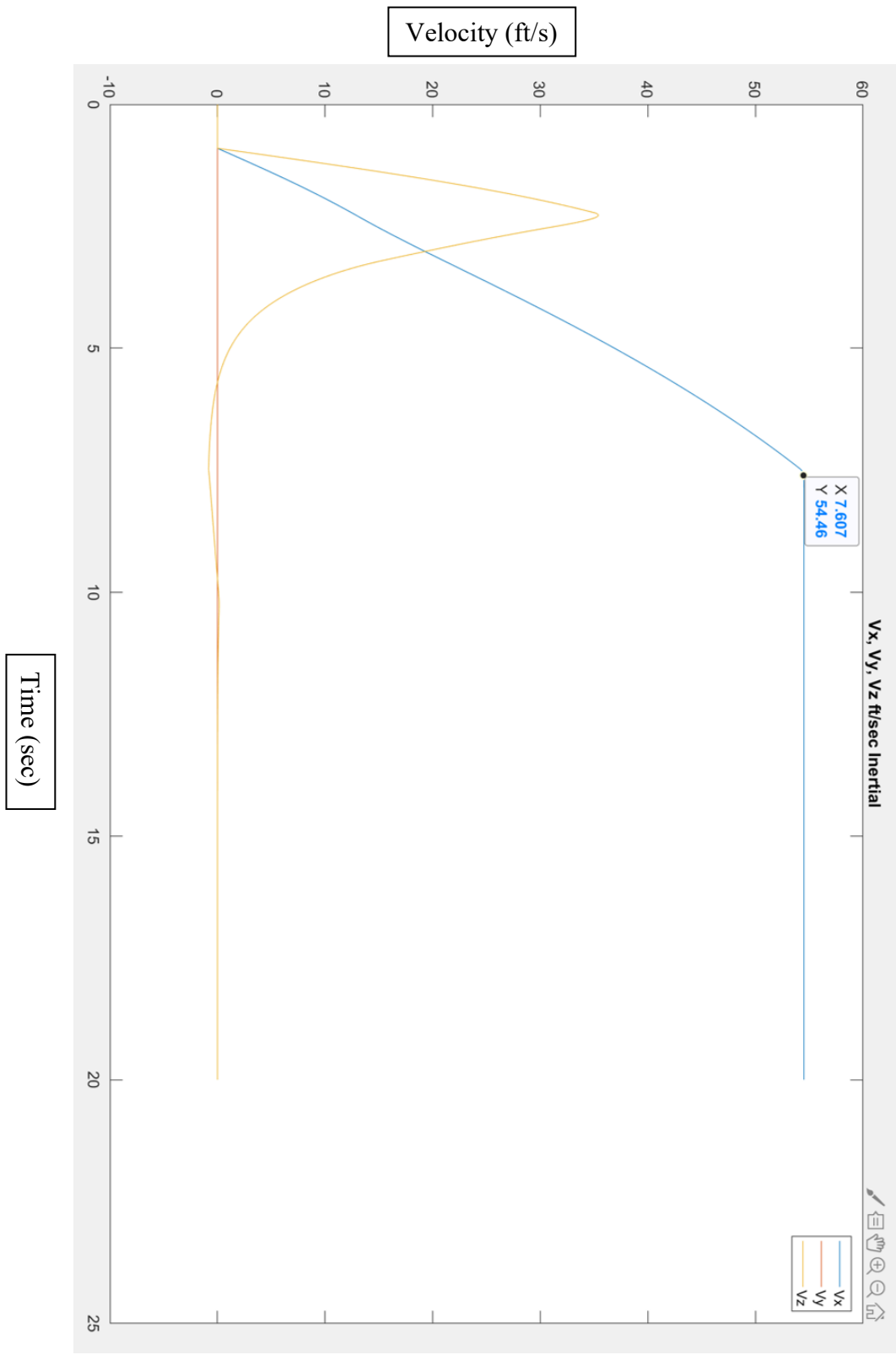


Figure 5.14: Flat Free-Fall Transition Velocities

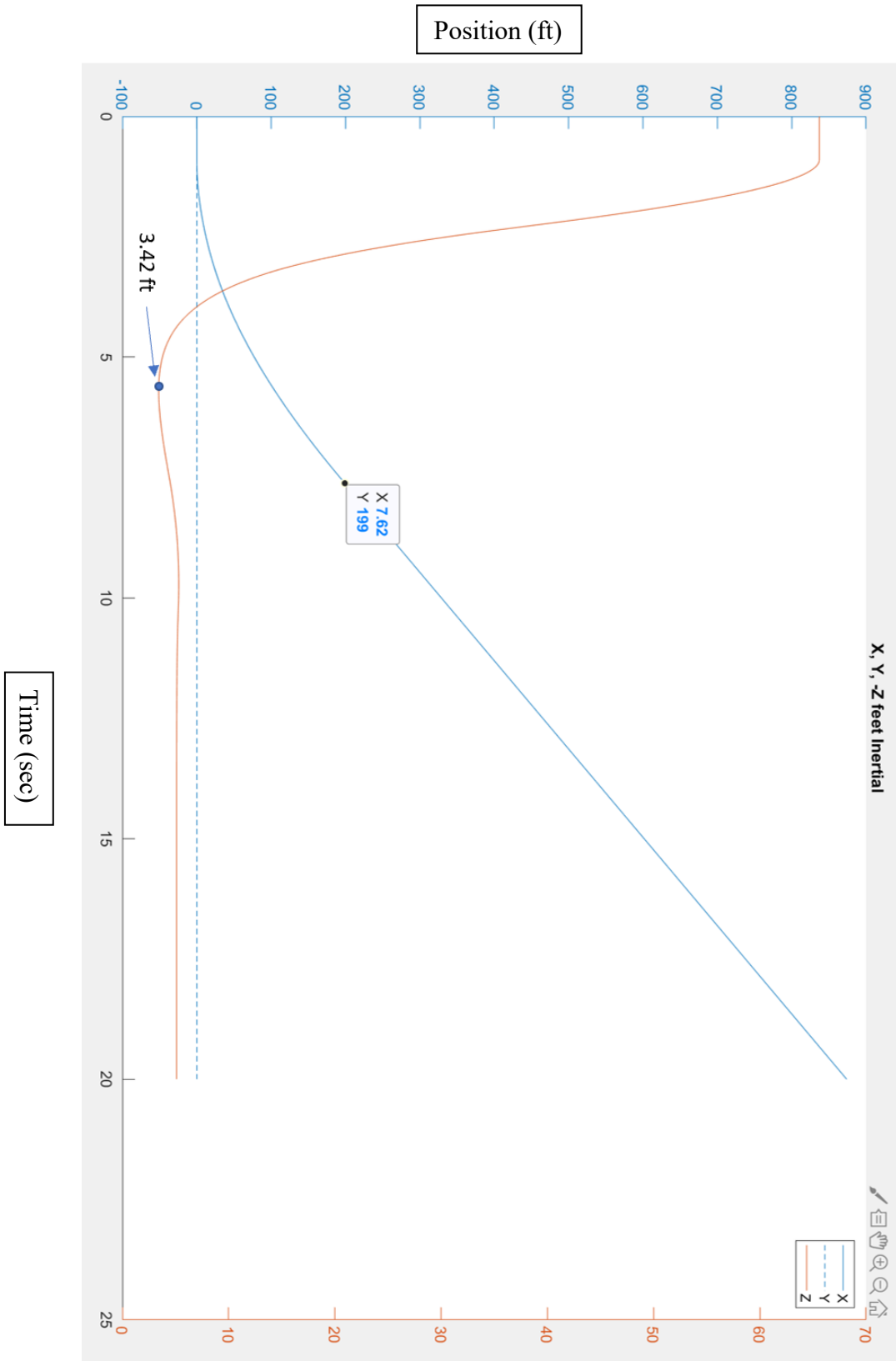


Figure 5.15: Flat Free-Fall Transition Positions

### 5.1.6 Nose-Dive Transition (Decrease in Altitude)

The next transition that I have simulated is more of a nose-dive transition. For this transition, there were some limitations to it. One of them was that based on the wing profile that the Albatross UAV uses, I only had coefficient values from an AOA of  $-11.25^\circ$  to  $14.5^\circ$ . Another limitation was the velocity that the UAV was able to get up to. The lower the AOA that was wanted to use for the nose-dive transition, the more required velocity. So for this transition, the lowest AOA that was able to be used was  $-0.5^\circ$ , or a pitch angle of  $-7.5^\circ$ . The last limitation to make this transition successful was needing to start at a lower altitude. The initial conditions were 50 feet in altitude and 0 ft/sec in the forward-moving direction, but with the desired conditions of 5 feet in altitude with 109.04 ft/sec in the forward-moving velocity. The control error values remained the same.

The forces in the nose-dive transition are then shown in Figure 5.16. For the force in this transition, rotors 1 through 4 start with forces of 5.5 lbs each and go to 0 lbs. to show that the hover rotors were shut off, and rotor 5 starts at the maximum. Quickly, the control picks up that a torque in the x-axis was being produced from the FW rotor, and rotors 2 and 3 start producing a force to counteract it for some time before decreasing along with the FW rotor. The UAV fully obtains flight and reaches the desired speed in the x-direction at about 5.55 sec. as shown in Figure 11.9. The velocity in the y-direction remains at 0 ft/sec and the velocity in the z-direction slightly fluctuates before stabilizing at 0 ft/sec as well. Figure 5.18 shows the positions of the UAV. In red shows the position in the z-direction that better shows the fluctuations of the velocity in the z-direction. When starting at an altitude of 50 feet, the UAV slightly overshoots the desired altitude down to about 0.37 feet and then reaches 10 feet before stabilizing at the desired altitude. The

position in the y-direction remains at 0 and the position in the x-direction gets to about 613.1 feet until the transition is completed.

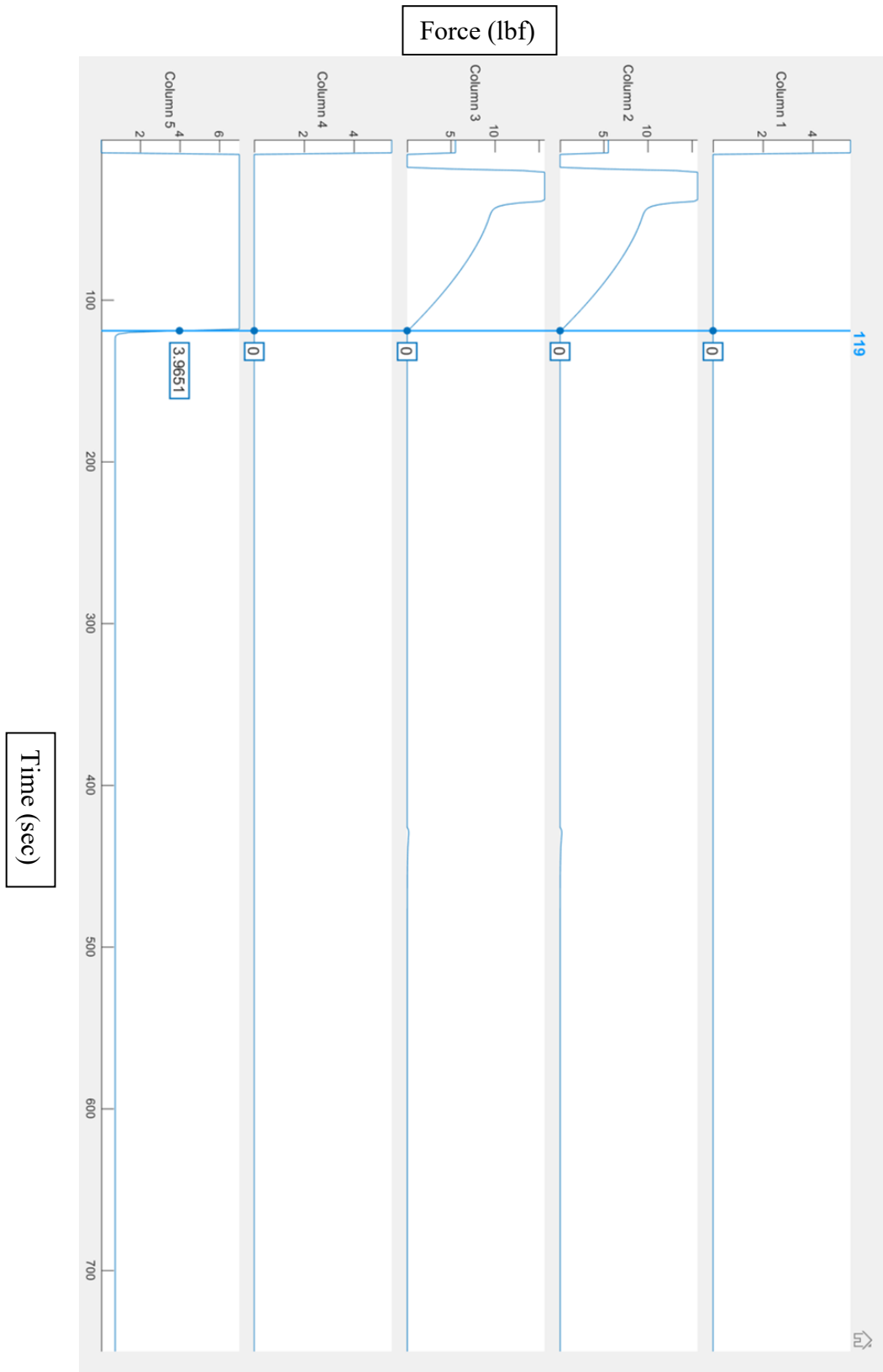


Figure 5.16: Nose-Dive Transition Forces

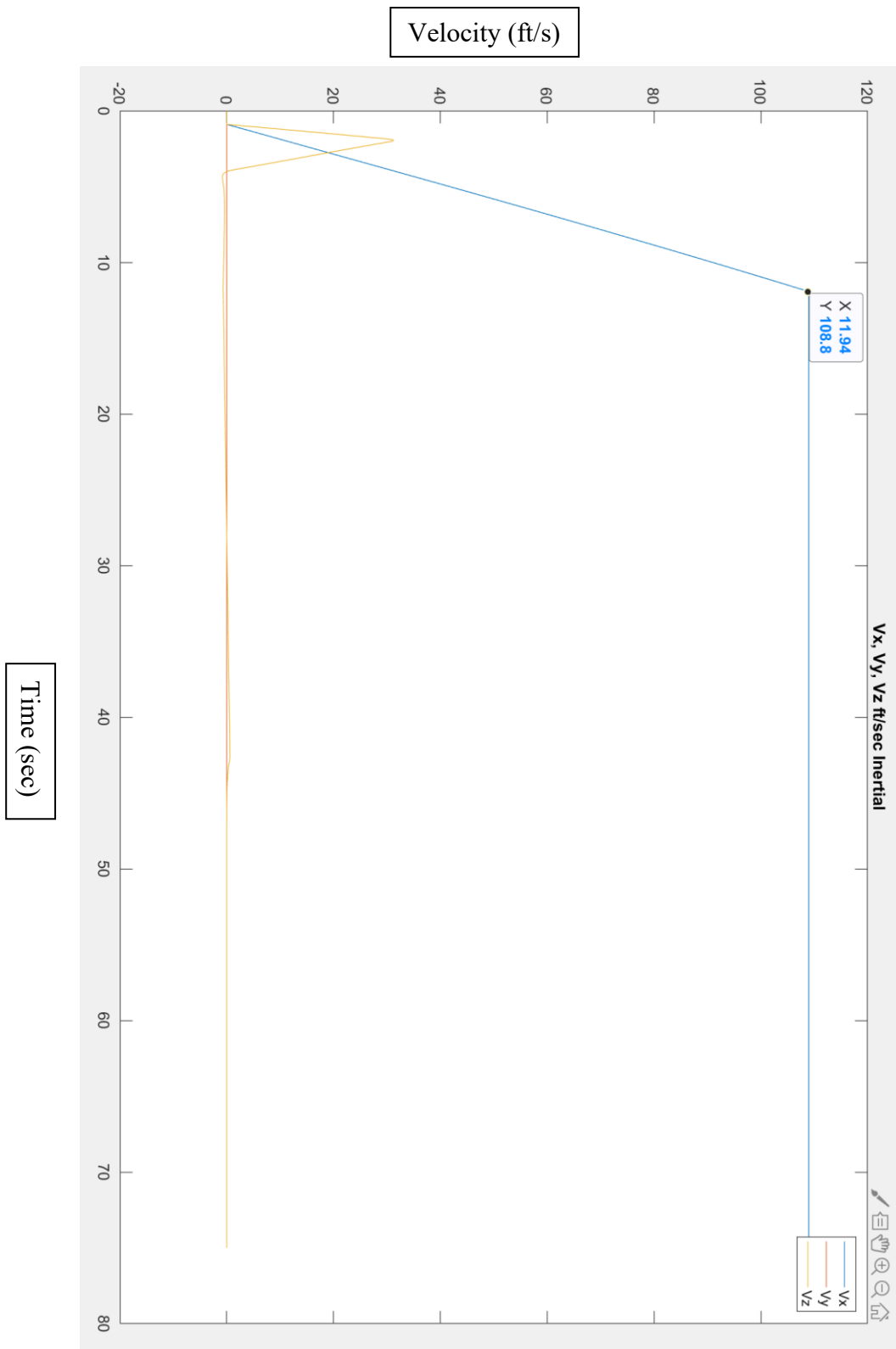


Figure 5.17: Nose-Dive Transition Velocities

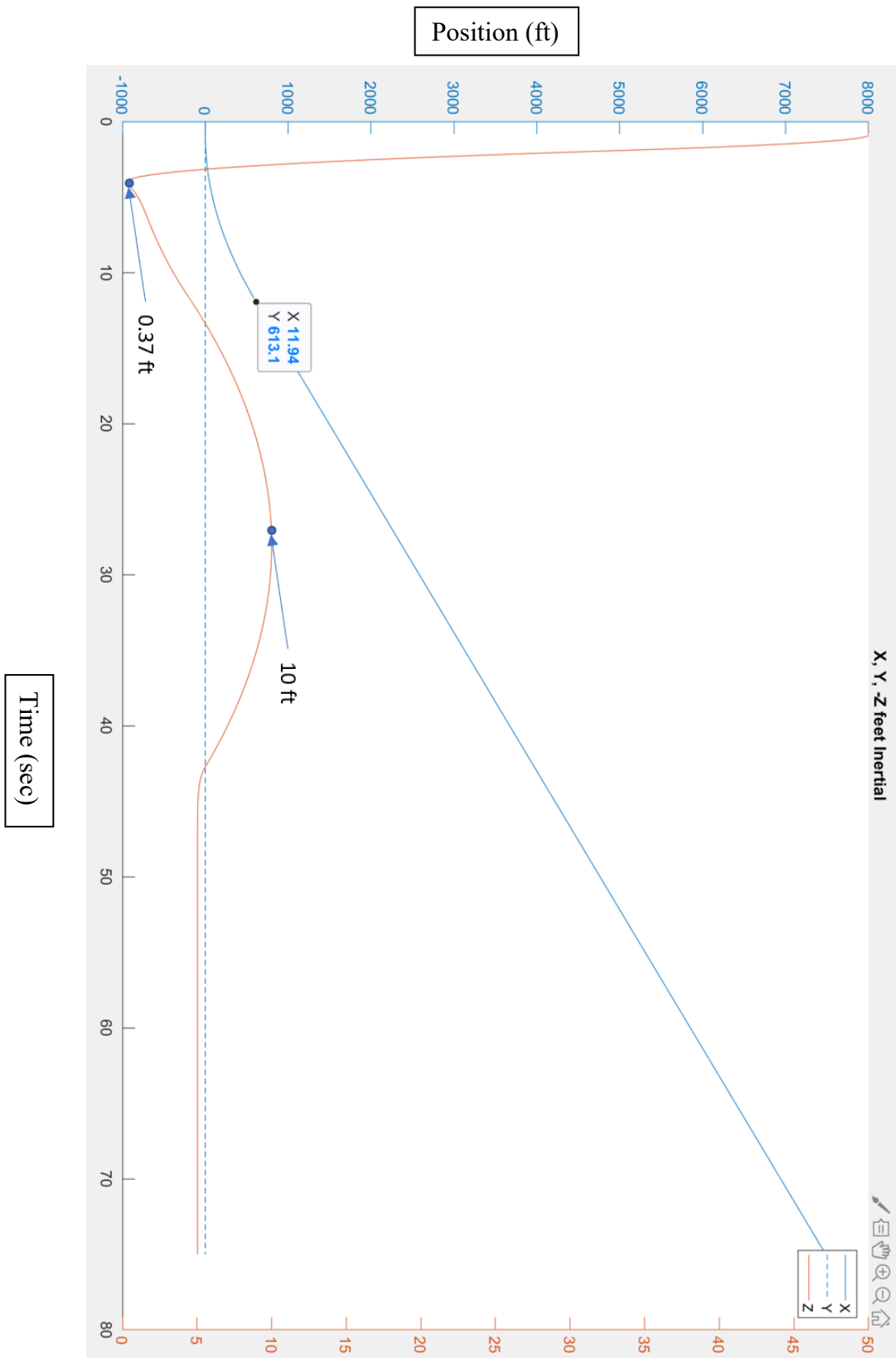


Figure 5.18: Nose-Dive Transition Positions

## 5.2 FIXED-WING TO HOVER TRANSITIONS

### 5.2.1 Reverse Thrust Transition

To start with the backwards transition, the first simulation uses conditions of the baseline backwards transition that is normally done with the Dronecode flight control software. For these simulations, they will each be starting in the middle of flight for 1 sec before the transitions begin. The initial conditions of the UAV had FW flight at 65.6 feet in altitude, 54.8 ft/sec velocity in the forward-moving direction, and  $0^\circ$  of the pitch. The desired conditions were to remain at 65.6 feet in altitude and reach 0 ft/sec while remaining at  $0^\circ$  of the pitch. This reverse thrust transition is simulated by stopping the FW rotor from producing forward thrust and start to produce reverse thrust, and turning on the hover rotors at the same time. The control error values remained the same.

From the forces in the reverse thrust transition shown in Figure 5.19, the four hover rotors are getting up to about 5.5 lbs each, which is what is needed to stabilize the hover for the 22 lb. Albatross UAV. This time for the backwards transition, rotors 1 and 4 are the ones producing more force than rotors 2 and 3, and the reason for that is because now we are producing a backwards thrust from the FW rotor. This means that it is spinning in the opposite direction, which is counterclockwise, and producing a torque in the clockwise direction. Therefore motors 1 and 4, being on the right side of the UAV, produce more thrust to stabilize the UAV. As the UAV is getting closer to the desired velocity of 0 ft/sec, the backwards thrust of the FW rotor is starting to go to 0 lbs, and the hover rotors are stabilizing at 5.5 lbs.

The velocities in Figure 5.20 shows the Albatross fully completing the transition back to hover with a forward-moving velocity of 0 ft/sec at roughly 6.1 sec. The velocity in the y-direction remains at 0 ft/sec, and the velocity in the z-direction slightly fluctuates before stabilizing at 0

ft/sec as well. Figure 5.21 shows as the backwards transition is occurring, the UAV traveled about 173 feet of distance in the x-direction before coming to a complete stop. Because there is still a forward moving velocity and the four hover rotors are activated as well, there was a slight gain in altitude to 66.63 feet in the z-direction before stabilizing at the desired 65.6 feet.

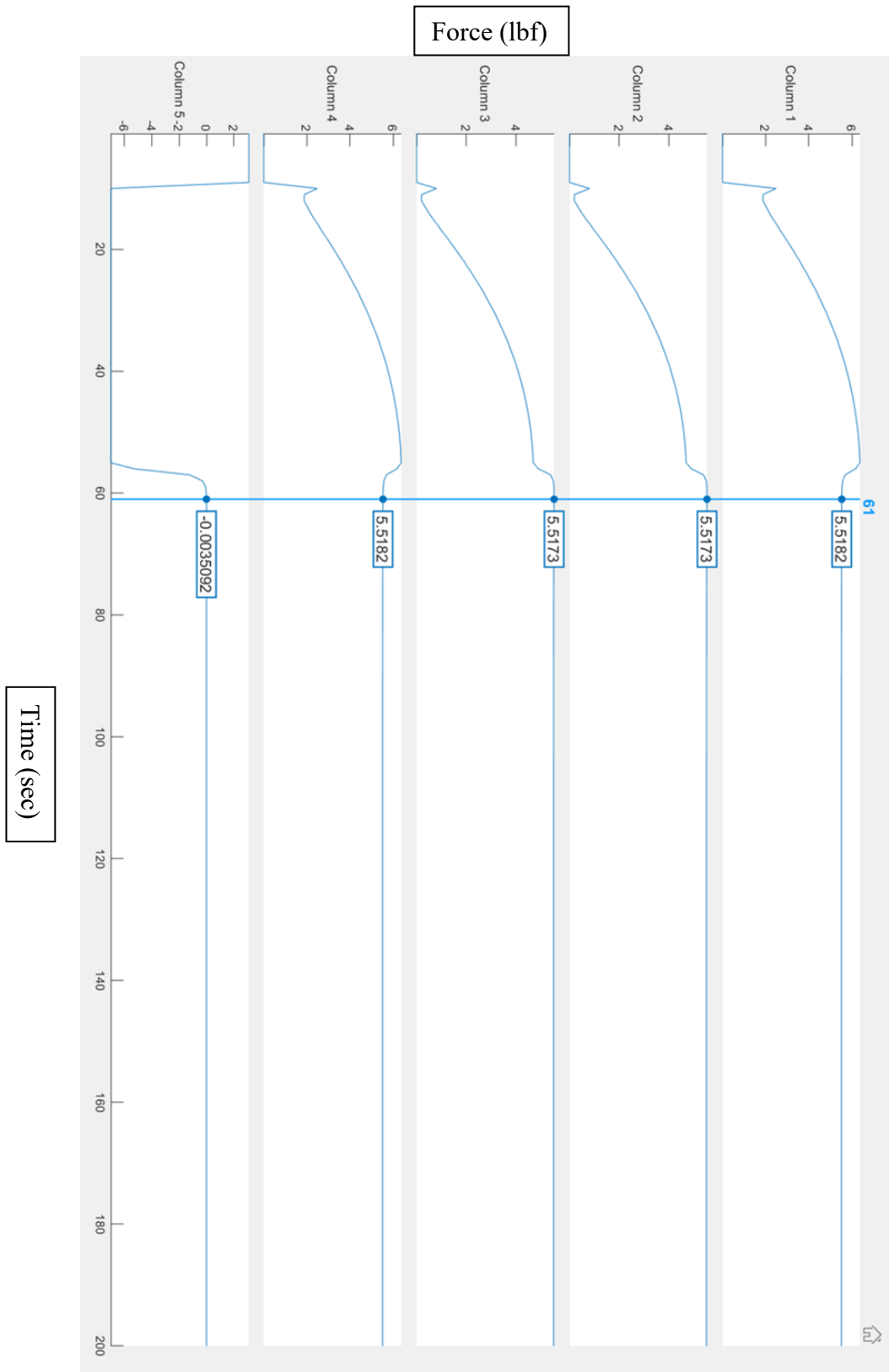


Figure 5.19: Reverse Thrust Transition Forces

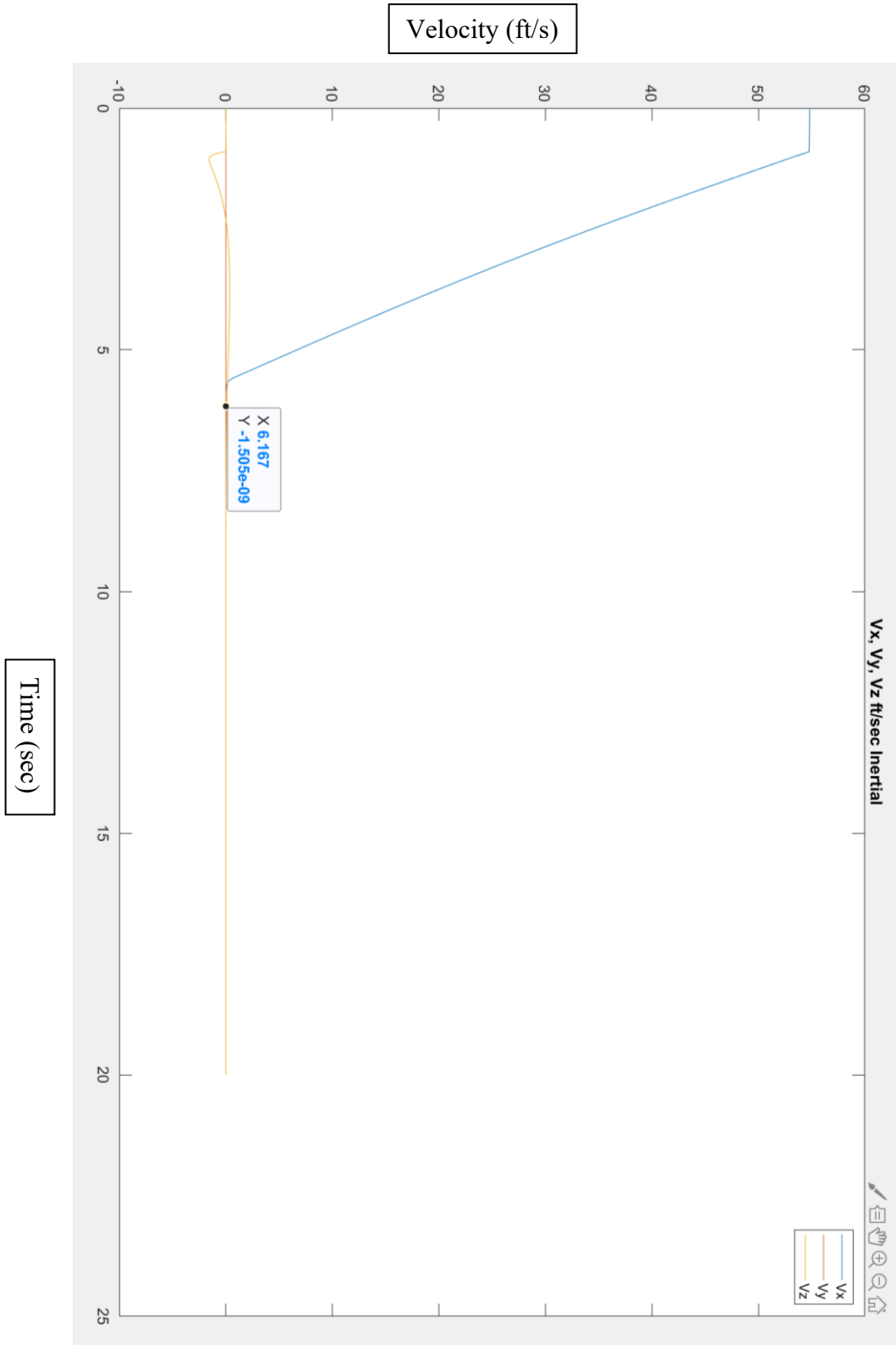


Figure 5.20: Reverse Thrust Transition Velocities

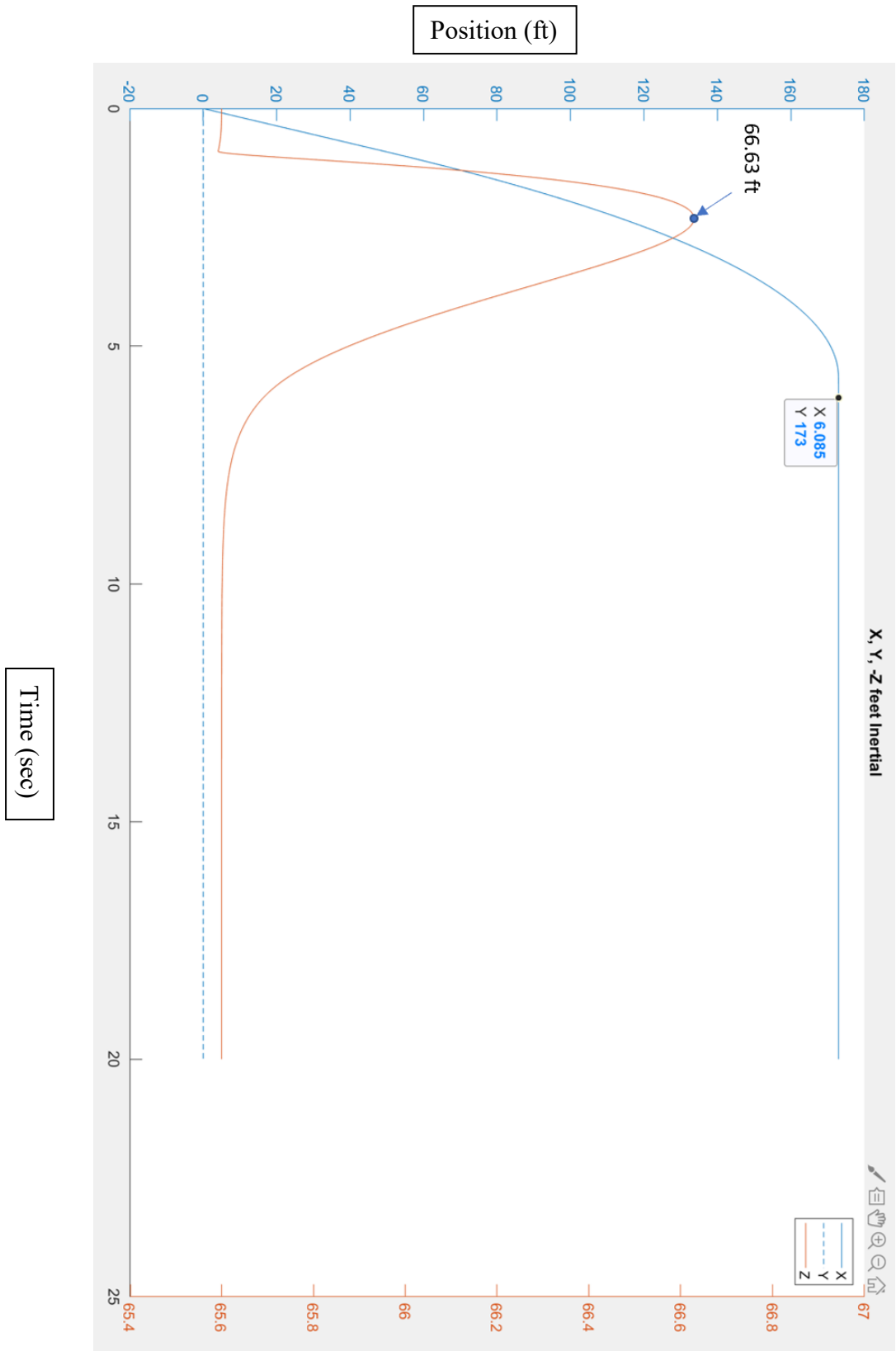


Figure 5.21: Reverse Thrust Transition Positions

### 5.2.2 Flat Gliding Transition

Another transition was simulated by just shutting off the FW rotor and turning on the hover rotors, and letting the Albatross glide until full control of hover mode was obtained. This trial for the backward transition is different than the reverse thrust transition. The initial conditions of the UAV had FW flight at 65.6 feet in altitude, 54.8 ft/sec velocity in the forward-moving direction, and  $0^\circ$  of the pitch. The desired conditions were to remain at 65.6 feet in altitude and reach a 0 ft/sec velocity while remaining at  $0^\circ$  of the pitch. The control error values remained the same.

From Figure 5.22, when the FW rotor is shut off, the hover rotors are activated, but then hold back at the very next time step because, at the beginning of the transition, there is still a lift force being produced from the wings from the initial velocity. The hover rotors start to hold back for a brief moment before starting to pick back up again as the velocity is slowing down. Not as much lift force is being provided. The forces in the four hover rotors are slowly increasing, but it does take a while for them to hit 5.5 lbs. exactly because there is still a small forward moving velocity from the UAV since it is gliding. That forward moving velocity is still causing a bit of lift from the wings, and that is why they are not at 5.5 lbs within this time frame.

Figure 5.23 shows the velocities of the UAV. The velocity in the x-direction is shown in blue. From looking into the average velocities of a quadcopter to still have full control in hover mode, that velocity was about 3.25 ft/sec. The transition was determined once the UAV had reached that velocity because waiting for the UAV to reach exactly 0 ft/sec would take too long. This transition reaches that speed at about 190 sec, so that is when the hover rotors have full control of the UAV from the transition from FW flight to hover. The red shows the velocity in the y-direction, which remains at a value of zero, and the yellow shows the velocity in the z-direction. Looking closely, a very minor increase of the z-velocity in the negative z-direction because the

force being provided by the hover rotors at the very start is being added with the amount of lift that is being produced by the wings and the FW rotor, but quickly returns to a z-velocity of 0 ft/sec.

For the positions of this backwards transition in Figure 5.24, starting with the z-position to show the results of the forces from the hover rotors combined with the lift from the wings and FW rotor in the very beginning of the simulation shows a gain in altitude. Because for a very brief moment, they provide a total force in the negative z-direction of slightly more than 22 lbs., there is a slight gain in altitude to roughly 67.2 feet but quickly returns to the desired altitude of 65.6 feet. For the y-position, that value remains at zero, and for the x-position, because it takes 190 sec to get full control in hover mode, the UAV cruises forward to a distance of about 1900 feet.



Figure 5.22: Flat Gliding Transition Forces

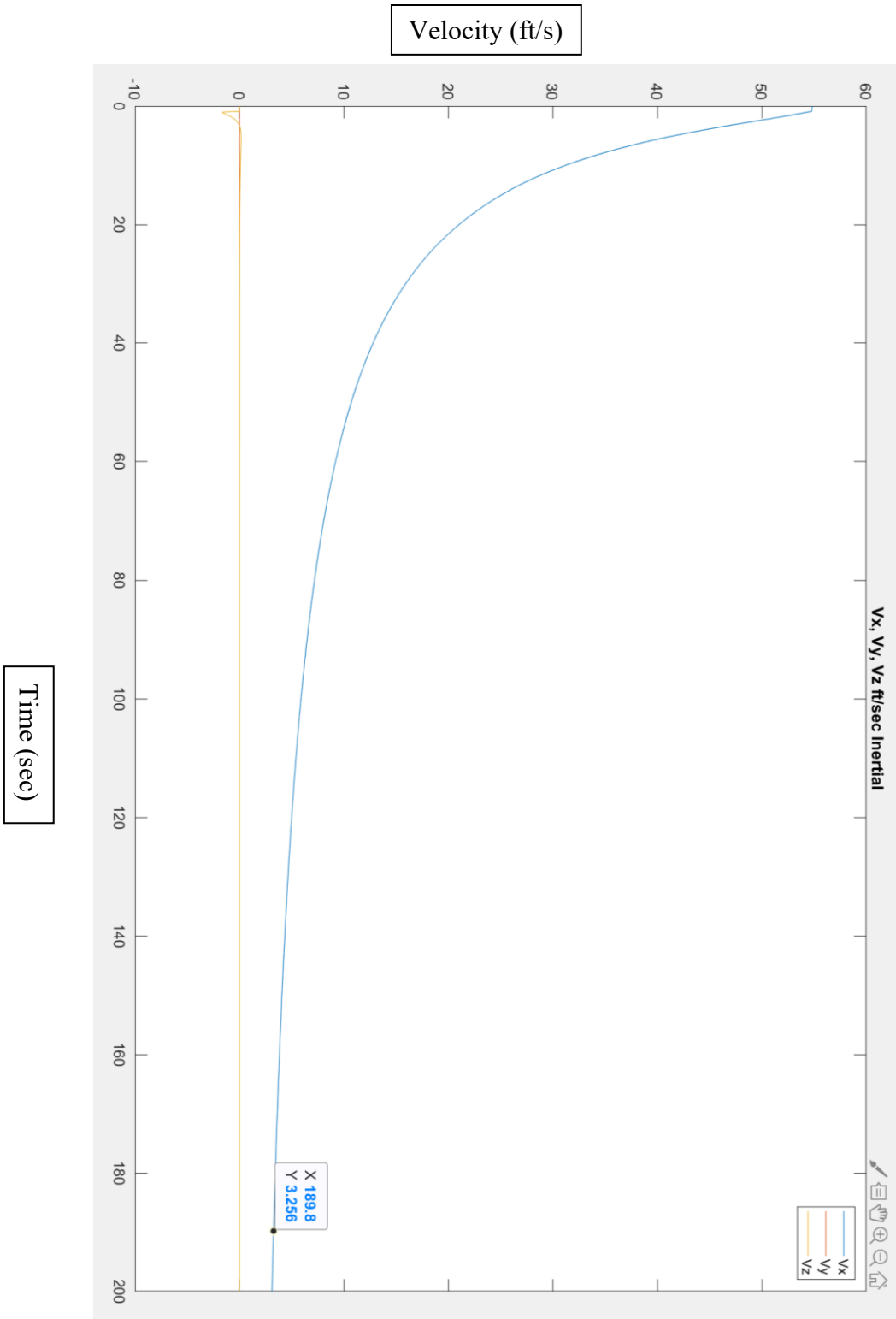


Figure 5.23: Flat Gliding Transition Velocities

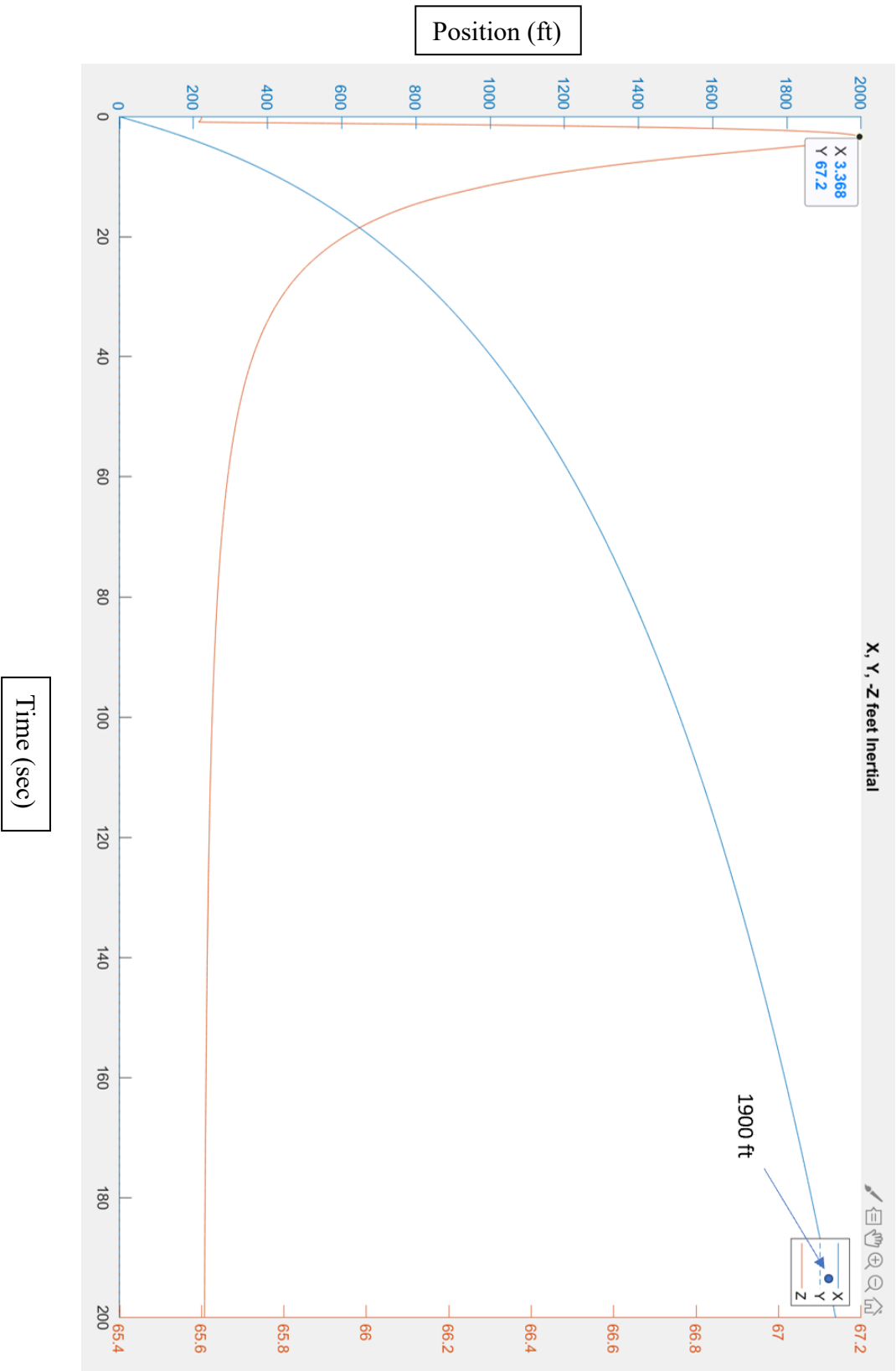


Figure 5.24: Flat Gliding Transition Positions

### 5.2.3 Pitched-Back Gliding Transition

With the gliding pitched-back transition, the initial conditions of the UAV were again having FW flight at 65.6 feet in altitude, 54.8 ft/sec velocity in the forward-moving direction, and 0 degrees of pitch. The desired conditions were to have a forward velocity of 0 ft/sec, remain at an altitude of 65.6 feet, and use a pitch angle of  $4^\circ$ , giving us an AOA of  $11^\circ$ , which is right below the critical AOA to prevent a stall from happening during this transition. The control error values remained the same.

With Figure 5.25 showing the forces in all of the rotors, once again, rotors 1 through 4 get a value very close to 5.5 lbs. each because there is still a very small forward moving velocity even though it shows 0 lbs. of force being provided from the FW rotor. Figure 5.26 shows the velocities of the UAV and using the same information gathered as to when it will have full control of the UAV for hover mode when reaching a speed of 3.25 ft/sec, this transition shows that the velocity in the x-direction, shown in blue, reaches that speed at roughly 91 sec. The velocity in the y-direction shows a value of 0 ft/sec, while the velocity in the z-direction shows a few spikes again prior to stabilizing after a bit of time to 0 ft/sec.

For the positions of this transition in Figure 5.29, the z-position, in red, better shows the spikes that were occurring in both the forces and velocities. Because we are using an AOA value of  $11^\circ$ , combined with the initial velocity at the start of this transition, this causes lift in the UAV to occur. This shows this gain in altitude in the negative z-direction up to 80.5 feet. As the velocity is decreasing, the lift is decreasing as well, and the UAV begins to descend to the desired altitude of 65.6 feet. As all of that is occurring, the hover rotors are producing more and more force and reach their values of 5.5 lbs each. There is no change in the y-direction, and by the time the UAV fully gains control while hovering, it has traveled about 915 feet in the x-direction.

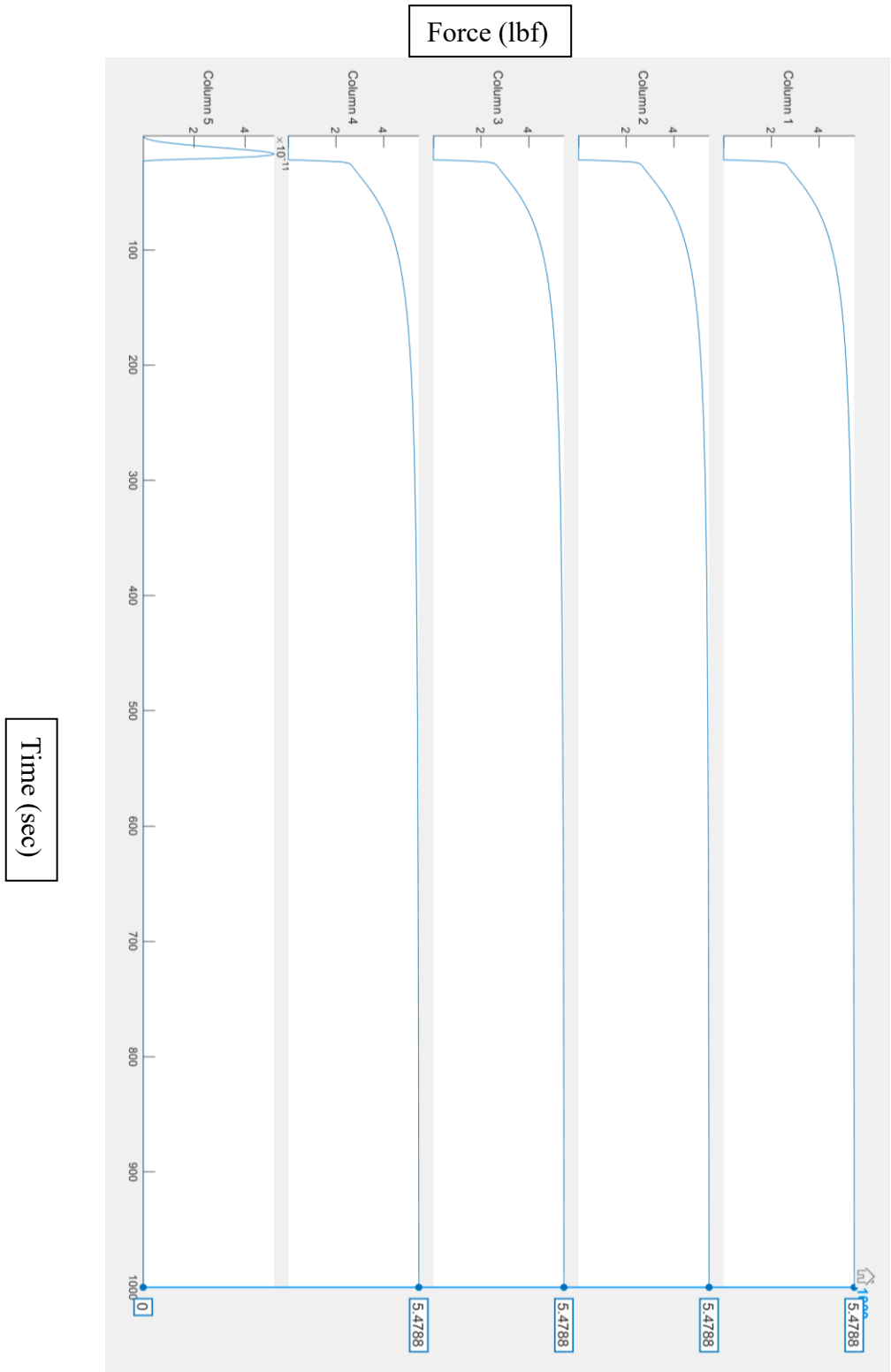


Figure 5.25: Pitched-Back Gliding Transition Forces

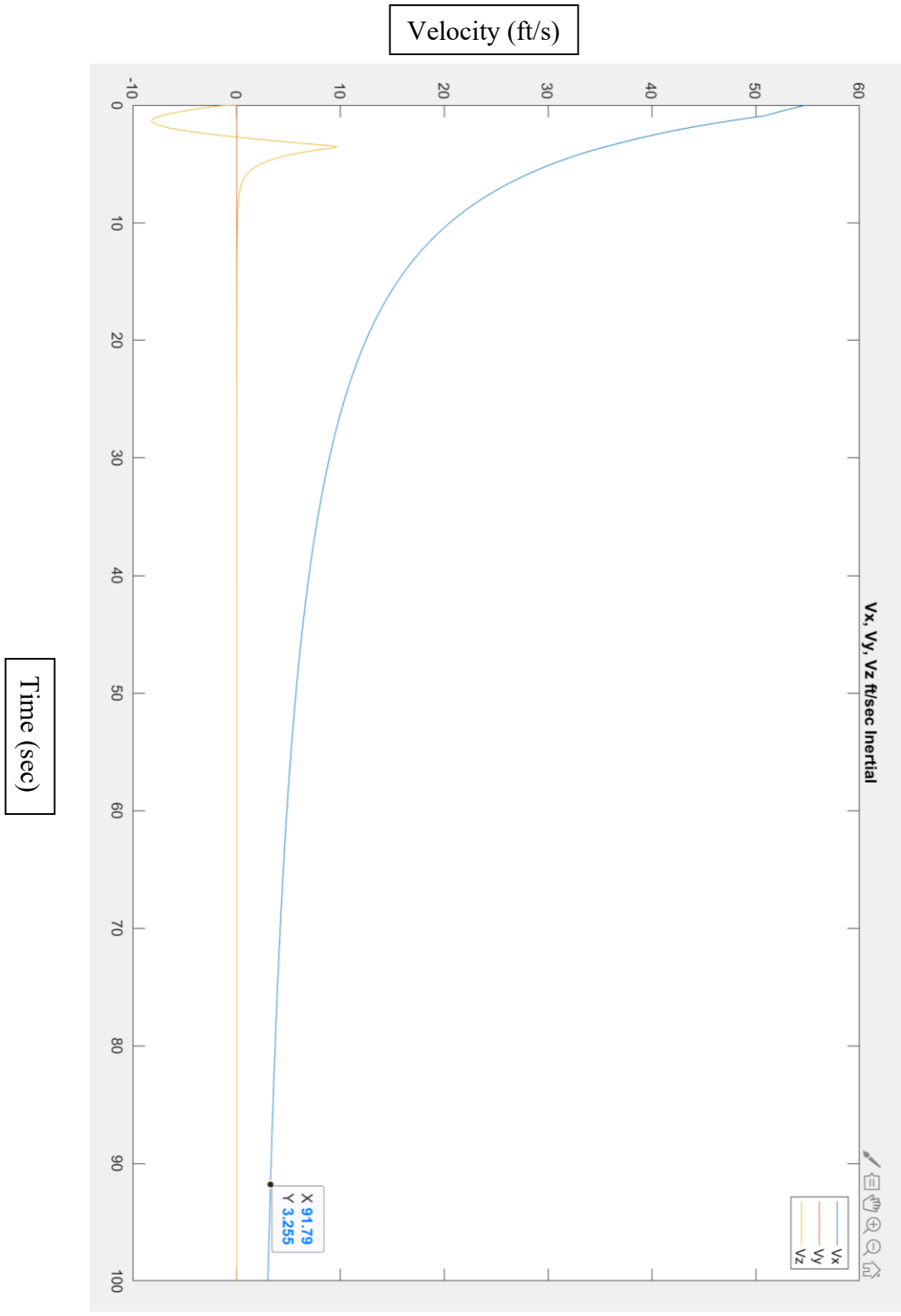


Figure 5.26: Pitched-Back Gliding Transition Velocities

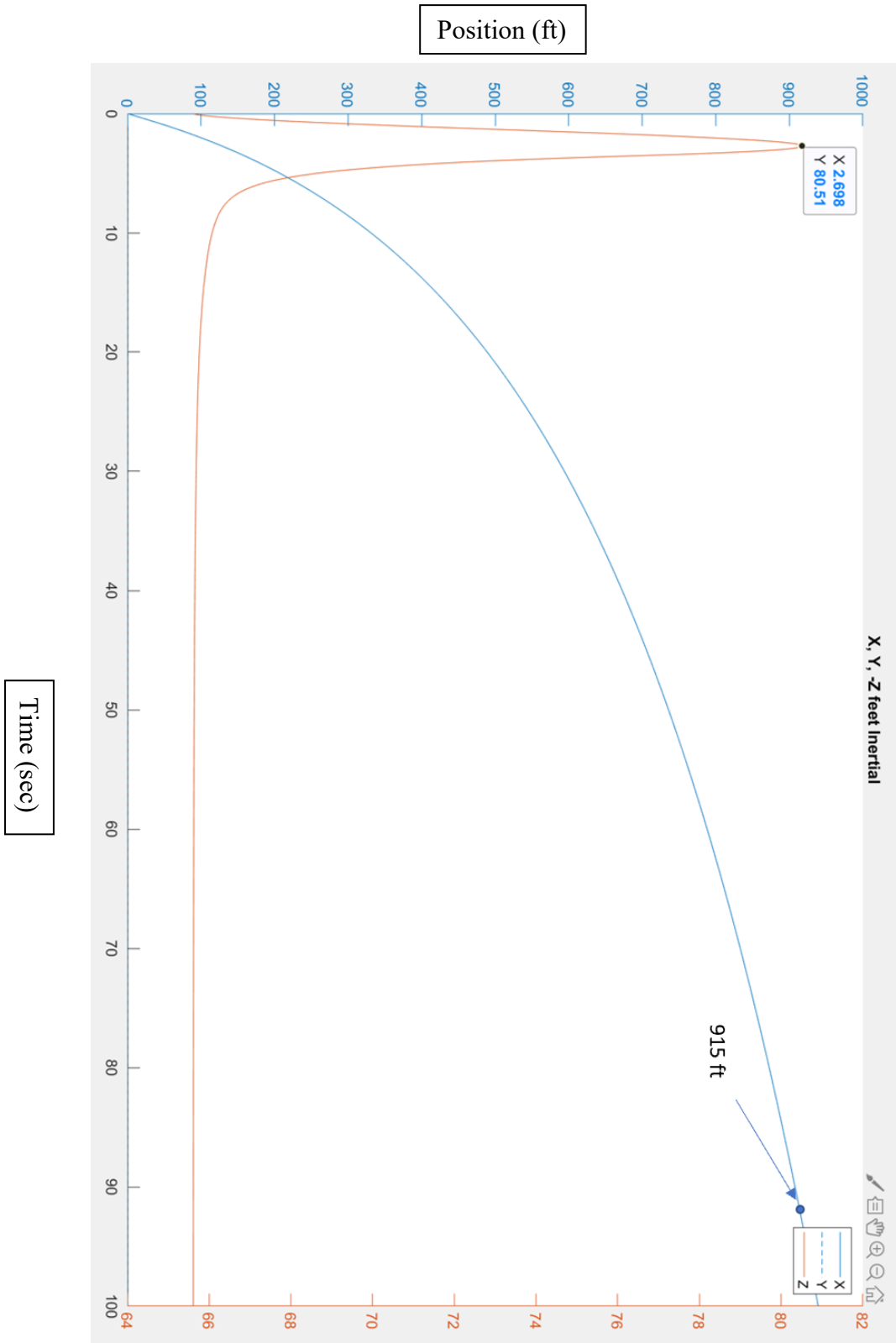


Figure 5.27: Pitched-Back Gliding Transition Positions

## Chapter 6: Conclusion

Table 6.1 shows the different hover to fixed-wing transitions that were simulated for this study. Because each transition started with hovering for 1 sec, the amount of force during that time was subtracted when calculating for the efficiencies. From the table, transitions 1 and 2 obtained flight in the least amount of time (7.4 sec), while transition 6 took the longest (11.9 sec). Transitions 1, 3, and 4 each had no loss in altitude (0 ft), as shown in the simulations. In comparison, transition 5 showed the most altitude loss (62.18 ft). The transition with the largest gain in altitude showed to be transition 4 when using the Optimum Angle of Attack (AOA) (2.75 ft). Of all of the hover to fixed-wing transitions, transition 5 seemed to have the least total amount of impulse (127.92 lbf\*s), while transition 6 showed the most impulse (234.51 lbf\*s).

Table 6.2 compares the three fixed-wing to hover transitions were done. Just like for table 6.1, because each transition was in FW flight for 1 sec before the transition occurred, the amount of force during that time was subtracted when calculating for the efficiencies. Transition 7 simulated having the least amount of time to transition from FW mode to hover mode (6.1 sec) while transition 8 simulated the complete transition to hover mode at about 31 times greater (190 sec). None of the transitions showed any altitude loss. For altitude gain, transition 7 showed the least amount (1.03 ft), while transition 9 showed the most (14.9 ft). Transition 7 also showed the least amount of impulse (114.58 lbf\*s) needed to complete the transition. Transition 8 showed the most (3889.41 lbf\*s).

Every transition simulated in this study was successful. For the hover to FW transitions, the baseline transition would best be used if not wanting to lose any altitude during the transition and also as being used as one of the quickest transitions. The flat transition can be used to maintain the UAV as close to the initial and desire conditions while going from hover to FW flight mode.

The pitched-back transition may be used when not much velocity in the UAV is wanted, and the pitched-forward transition would best be used by the Remote Pilot in Command when wanting to gain the most altitude during the transition since that method uses the Optimum AOA. As far as the most efficient transition, the flat free-fall would be the best choice, and the transition that is not recommended because the flight time was the longest and the least efficient is the nose-dive transition. Both of these transitions could also be used in the case the hover rotors are shut off, it would still be possible to recover with a transition to FW flight. This will be able to save the UAV from crashing into the ground. As far as the FW to hover transitions, the reverse thrust transition is best used when wanting to do the shortest transition, least amount of altitude gained during the transition, and the most efficient. If wanted to maintain high velocities during the transition or even if the FW battery can no longer be used, the two gliding transitions would be preferred.

Future work for this study would be the following to focus on:

- Controller tuning
- Different controllers other than the PD controller used for this study
- Different motor/propeller selections
- Drag of irregular objects should anything else be implemented to the UAV
- Implement study to flight simulator
- Implement study to physical Albatross UAV

Table 6.1: Hover to Fixed-Wing Transition Comparison

	<b>Transition</b>	<b>Obtained Flight (sec)</b>	<b>Altitude Loss During Transition (ft)</b>	<b>Altitude Gain During Transition (ft)</b>	<b>Required Hover Impulse (lbf*s)</b>	<b>Required FW Impulse (lbf*s)</b>	<b>Total Required Impulse (lbf*s)</b>
1	Baseline  (No Altitude Loss)	7.4	0	2.54	85.58	44.65	130.24
2	Flat (Same Altitude)	7.4	1.98	0.34	86.19	44.65	130.84
3	Pitched- Back	7.8	0	2.2	82.47	47.42	129.89
4	Pitched- Forward	7.7	0	2.75	92.64	46.71	139.35
5	Flat Free- Fall	7.6	62.18	0	81.85	46.07	127.92
6	Nose-Dive	11.9	49.63	0	158.16	76.35	234.51

Table 6.2: Fixed-Wing to Hover Transition Comparison

	<b>Transition</b>	<b>Obtained Hover (sec)</b>	<b>Altitude Loss During Transition (ft)</b>	<b>Altitude Gain During Transition (ft)</b>	<b>Required Hover Impulse (lbf*s)</b>	<b>Required FW Impulse (lbf*s)</b>	<b>Total Required Impulse (lbf*s)</b>
7	Reverse Thrust	6.1	0	1.03	82.04	32.54	114.58
8	Flat Gliding	190	0	1.6	3889.41	0	3889.41
9	Pitched- Back Gliding	91	0	14.9	1831.47	0	1831.47

## References

1. (Airfoil Tools, n.d.) Airfoil Tools. (n.d.). Retrieved October 24, 2020, from <http://www.airfoiltools.com/polar/details?polar=xf-naca2410-il-200000>
2. (Albatross Airframe, n.d.) Albatross Airframe. (n.d.). Retrieved October 22, 2020, from <http://store.appliedaeronautics.com/albatross-airframe/>
3. (Angelofski, 2018) Angelofski, S. (2018). Medical Drones are Saving Lives in Africa. Retrieved 2018, from <https://thedronesworld.net/medical-drones-are-saving-lives-in-africa/>
4. (Apkarian, 2017) Apkarian, J. (2017). Pitch-decoupled VTOL/FW aircraft: First flights. *2017 Workshop on Research, Education and Development of Unmanned Aerial Systems (RED-UAS)*.
5. (Basson, 2010) Basson, M. M. (2010). *Stall Prevention Control of Fixed-Wing Unmanned Aerial Vehicles*.
6. (Bushgens & Sukhanov, 2018) Bushgens, G. S., & Sukhanov, V. L. (2018). Concept Of A Modern Fighter. *TsAGI Science Journal*, 49(4), 343-359.
7. (Çakici & Leblebicioğlu, 2016) Çakici, F., & Leblebicioğlu, M. K. (2016). Control System Design of a Vertical Take-off and Landing Fixed-Wing UAV. *IFAC-PapersOnLine*, 49(3), 267-272.
8. (Çakici & Leblebicioğlu, Analysis of a UAV that can Hover and Fly Level, 2016) Çakıcı, F., & Leblebicioğlu, M. K. (2016). Analysis of a UAV that can Hover and Fly Level. *MATEC Web of Conferences*, 59, 07010. doi:10.1051/mateconf/20165907010
9. (Can Thermal Imaging See Through Walls? And Other Common Questions, 2020) Can Thermal Imaging See Through Walls? And Other Common Questions. (2019). Retrieved

October 24, 2020, from <https://www.flir.com/discover/cores-components/can-thermal-imaging-see-through-walls/>

10. (Collins, 2020) Collins, D. (2020, May 26). Motion basics: How to define roll, pitch, and yaw for linear systems. Retrieved October 24, 2020, from <https://www.linearmotiontips.com/motion-basics-how-to-define-roll-pitch-and-yaw-for-linear-systems/>
11. (Diebel, 2006) Diebel, J. (2006). *Representing Attitude: Euler Angles, Unit Quaternions, and Rotation Vectors*.
12. (Dundar, Bilici, & Ünler, 2020) Dündar, Ö, Bilici, M., & Ünler, T. (2020). Design and performance analyses of a fixed wing battery VTOL UAV. *Engineering Science and Technology, an International Journal*. doi:10.1016/j.jestch.2020.02.002
13. (Dydek, Annaswamy, & Lavretsky, 2013) Z. T. Dydek, A. M. Annaswamy and E. Lavretsky, "Adaptive Control of Quadrotor UAVs: A Design Trade Study With Flight Evaluations," in *IEEE Transactions on Control Systems Technology*, vol. 21, no. 4, pp. 1400-1406, July 2013.  
doi: 10.1109/TCST.2012.2200104
14. (Flying a Quadplane, n.d.) Flying a QuadPlane¶. (n.d.). Retrieved November 23, 2020, from <https://ardupilot.org/plane/docs/quadplane-flying.html>
15. (Forces in a Climb, n.d.) Forces in a Climb. (n.d.). Retrieved October 24, 2020, from <https://www.grc.nasa.gov/WWW/K-12/airplane/climb.html>
16. (Govdel, Muzaffar, Raj, Elhadidi, & Kayacan, 2019) Govdeli, Y., Muzaffar, S. M., Raj, R., Elhadidi, B., & Kayacan, E. (2019). Unsteady aerodynamic modeling and control of

- pusher and tilt-rotor quadplane configurations. *Aerospace Science and Technology*, 94, 105421.
17. (Guo & Horn, 2012) Guo, W., & Horn, J. (2006). Modeling and Simulation for the Development of a Quad-Rotor UAV Capable of Indoor Flight. *AIAA Modeling and Simulation Technologies Conference and Exhibit*. doi:10.2514/6.2006-6735
  18. (Jamal, 2018) Jamal, A. (2018, January 03). What Does it Mean By Quadrotor: Unmanned Aerial Vehicles (UAVs). Retrieved October 22, 2020, from <https://www.electronicshobby.com/2017/11/what-does-it-mean-by-quadrotor-unmanned.html>
  19. (Jin-seo, 2007) Jin-seo, C. (2007, December 31). Tilt-Rotor Unmanned Plane to Become Smarter. Retrieved October 22, 2020, from [http://www.koreatimes.co.kr/www/news/tech/2009/10/129\\_16478.html](http://www.koreatimes.co.kr/www/news/tech/2009/10/129_16478.html)
  20. (Kim, et al., 2013) H. J. Kim et al., "Fully Autonomous Vision-Based Net-Recovery Landing System for a Fixed-Wing UAV," in *IEEE/ASME Transactions on Mechatronics*, vol. 18, no. 4, pp. 1320-1333, Aug. 2013.
  21. (Kim, Oh, Seo, & Kim, 2017) Kim, D., Oh, G., Seo, Y., & Kim, Y. (2017). Reinforcement Learning-Based Optimal Flat Spin Recovery for Unmanned Aerial Vehicle. *Journal of Guidance, Control, and Dynamics*, 40(4), 1076-1084.
  22. (Kloosterman, et al., 2019) Kloosterman, K., Doehler, D., Leichman, A., Barak, N., Staff, I., & Blum, B. (2014, January 29). The Waze of agriculture. Retrieved October 24, 2020, from <https://www.israel21c.org/the-waze-of-agriculture/>

23. (Kramer, 1932) Kramer, M. (1932). National Advisory Committee for Aeronautics.  
*Increase in the Maximum Lift of an Airplane Wing Due to a Sudden Increase in Its Effective Angle of Attack Resulting from a Gust.*
24. (Kubo, 2006) Kubo D. (2006). Study on Design and Transitional Flight of Tail Sitting VTOL UAV, *25th International Congress of the Aeronautical*, Hamburg, Germany.
25. (Lee, Giri, & Son, 2017) S. Lee, D. K. Giri and H. Son, "Modeling and control of quadrotor UAV subject to variations in center of gravity and mass," 2017 14th International Conference on Ubiquitous Robots and Ambient Intelligence (URAI), Jeju, 2017, pp. 85-90.
26. (Marchini, 2013) Marchini, B. D. (n.d.). Adaptive Control Techniques for Transition-to-Hover Flight of Fixed-Wing UAVs.
27. (Masuda & Uchiyama, 2018) Masuda, K., & Uchiyama, K. (2018). Robust Control Design for Quad Tilt-Wing UAV. *Aerospace*, 5(1), 17. doi:10.3390/aerospace5010017
28. (Performing Aerobatics Wreck, 2020) Performing Aerobatics Wreck. (2020). Retrieved October 24, 2020, from <https://zavodilov.ru/en/osnovnye-sredstva/vypolnenie-figur-vysshego-pilotazha-krushenie-ot-petli-do/>
29. (Quadplane Configuration, n.d.) QuadPlane Configuration. (n.d.). Retrieved October 24, 2020, from [https://docs.px4.io/master/en/config\\_vtol/vtol\\_quad\\_configuration.html](https://docs.px4.io/master/en/config_vtol/vtol_quad_configuration.html)
30. (Rotation Matrix, 2020) Rotation matrix. (2020, October 19). Retrieved October 24, 2020, from [https://en.wikipedia.org/wiki/Rotation\\_matrix](https://en.wikipedia.org/wiki/Rotation_matrix)
31. (Sanchez, Carrillo, Rondon, Lozano, & Garcia, 2010) Sanchez, A., Carrillo, L. R., Rondon, E., Lozano, R., & Garcia, O. (2010). Hovering Flight Improvement of a Quad-

rotor Mini UAV Using Brushless DC Motors. *Unmanned Aerial Vehicles*, 85-101.  
doi:10.1007/978-94-007-1110-5\_7

32. (Sujit, Saripalli, & Sousa, 2014) P. B. Sujit, S. Saripalli and J. B. Sousa, "Unmanned Aerial Vehicle Path Following: A Survey and Analysis of Algorithms for Fixed-Wing Unmanned Aerial Vehicless," in *IEEE Control Systems Magazine*, vol. 34, no. 1, pp. 42-59, Feb. 2014, doi: 10.1109/MCS.2013.2287568.
33. (Whalley, 1991) Whalley, M. S. (1991). Development and Evaluation of an Inverse Solution Technique for Studying Helicopter Maneuverability and Agility. *NASA Technical Memorandum*.
34. (Who's at Fault in a Multi-Car Accident?, 2018) Who's at fault in a multi-car accident?: Virginia Personal Injury Lawyers. (2018, October 19). Retrieved October 24, 2020, from <https://burnettwilliams.com/whos-at-fault-in-a-multi-car-accident/>
35. (Yu & Kwon, 2017) Yu, S., & Kwon, Y. (2017). Development of VTOL Drone for Stable Transit Flight. *Journal of Computer and Communications*, 05(07), 36-43.
36. (Yukse, Vuruskan, Ozdemir, Yukselen, & Inalhan, 2016). Yuksek, B., Vuruskan, A., Ozdemir, U., Yukselen, M. A., & Inalhan, G. (2016). Transition Flight Modeling of a Fixed-Wing VTOL UAV. *Journal of Intelligent & Robotic Systems*, 84(1-4), 83-105.
37. (Zhang, Chen, & Lv, 2012) Zhang, D., Chen, Z., & Lv, J. (2012). Lift System Design of Tail-Sitter Unmanned Aerial Vehicle. *Intelligent Control and Automation*, 03(04), 285-290. doi:10.4236/ica.2012.34033

## Vita

Born in Las Cruces, New Mexico, Luis Calvo made his way to El Paso, Texas before starting Franklin High School. Once graduated, he attended El Paso Community College for a couple of years before transitioning to The University of Texas at El Paso. While obtaining his bachelor's degree in Mechanical Engineering at the university, he had the opportunity to intern with an MEP firm in Phoenix, Arizona known as B&P Consulting Engineers. Upon graduating in the Fall of 2016, he began working full-time as a Mechanical Engineer at the engineering firm.

Shortly after, Luis decided to return to The University of Texas at El Paso to begin the master's graduate school program in the Fall of 2017. While obtaining his master's degree in Mechanical Engineering, Luis was a Mechanical Teaching Assistant for the mechanical department at the university. He transitioned to a Mechanical Research Associate during his final semester for his master's degree in the Fall of 2018 working for Dr. Michael McGee. Immediately after graduating with his master's degree, Luis began his Ph.D. studies in January 2019 with the MIRO Center for Space Exploration and Technology Research with Dr. Michael McGee and Dr. Louis Everett as his advisors. He interned with Lockheed Martin Space in both summers of 2019 and 2020 while completing his studies.

Also, during his Ph.D. studies, Luis presented a paper on "Mechanically Activated High-Temperature Synthesis" during the 2019 Southwest Emerging Technology Symposium. Plans were for him to present two other papers during the 2020 symposium on his research on "The Dynamic Transition of a Vertical Take-Off and Landing Drone" and "GPS Denied Environment with UAS Sensory Imagery," however, the event was canceled due to the COVID-19 pandemic.

Email: [calvo.luis@yahoo.com](mailto:calvo.luis@yahoo.com)

This dissertation was typed by Luis Calvo.